Vol. 9 No. 1 1988 ISSN: 0143-8166

OPTICS and LASERS in ENGINEERING

Edited by
F. P. CHIANG and G. T. REID

ELSEVIER APPLIED SCIENCE

OPTICS AND LASERS IN ENGINEERING

Optics and Lasers in Engineering aims to provide an international forum for the interchange of information on the development and application of optical techniques and laser technology in engineering. Emphasis is placed on contributions dealing with the practical use of methods and devices, the evaluation of results and development and enhancement of new or existing techniques. Attention is also given to the development of novel theoretical solutions and new theoretical foundations for experimental methods.

To reflect the main areas in which optical methods are being used and developed in an engineering environment, the scope of the journal is defined to include the following:

—Optical measurement techniques and transducers
—Photo-mechanics and opto-metrology
—Interferometry
—Optical methods for process control
—Opto-digital methods
—Applications of image processing
—Automated optical inspection and machine vision
—Optical nondestructive evaluation
—Applications of high powered lasers
—Laser safety.

Editors

PROFESSOR FU-PEN CHIANG
Laboratory for Experimental Mechanics Research,
State University of New York at Stony Brook,
Stony Brook, New York 11794-2300, USA

MR G. T. REID
Automation Division,
National Engineering Laboratory, East Kilbride,
Glasgow, Scotland G75 0QU, UK

Editorial Board

N. Abramson
Department of Production Engineering, The Royal Institute of Technology, Stockholm, Sweden

T. Asakura
Research Institute of Applied Electricity, Hokkaido University, Sapporo, Japan

F. N. Birkett
Department of Mechanical Engineering, Loughborough University of Technology, Loughborough, UK

K. Creath
WYKO Corporation, Tucson, Arizona, USA

F. L. Dai
Department of Engineering Mechanics, Tsinghua University, Beijing, People's Republic of China

R. Dändliker
Institute of Microtechnology, University of Neuchatel, Neuchatel, Switzerland

T. D. Dudderar
AT&T Bell Laboratories, Murray Hill, New Jersey, USA

J. S. Epstein
EG&G Idaho, Inc., Idaho Falls, Idaho, USA

C. Esposito
Centro Laser, Society Consortile srl, Bari, Italy

M. Halioua
Centre for Optics, Lasers and Holography, New York Institute of Technology, New York, USA

P. Hariharan
Division of Applied Physics, CSIRO, Lindfield, NSW, Australia

Y. Y. Hung
Center for Robotics and Advanced Automation, Dodge Hall of Engineering, Oakland University, Rochester, Michigan, USA

M. Idesawa
Information Science Laboratory, RIKEN: The Institute of Physical and Chemical Research, Wako, Saitama, Japan

O. J. Lokberg
Physics Department, The Norwegian Institute of Technology, Trondheim, Norway

J. R. Pekelsky
Photogrammetric Research Section, Division of Physics, National Research Council Canada, Ottawa, Canada

L. Pirodda
Department of Mechanical Engineering, University of Cagliari, Piazza d'Armi, Cagliari, Italy

M. Rioux
Photonics and Sensors Section, Division of Electrical Engineering, National Research Council Canada, Ottawa, Canada

D. W. Robinson
Division of Mechanical and Optical Metrology, National Physical Laboratory, Department of Trade & Industry, Middlesex, UK

B. F. Scott
Mechanical Engineering Department, University of Glasgow, Glasgow, UK

Y. S. Tan
Department of Mechanical Engineering, Xi'an Jiatong University, Xi'an, China

B. J. Thompson
University of Rochester, Rochester, New York, USA

B. Tozer
Lasermet Ltd, Brockenhurst, Hants, UK

J. D. Trolinger
SPECTRON Development Laboratories, Costa Mesa, California, USA

J. Tyrer
Department of Mechanical Engineering, Loughborough University of Technology, Loughborough, UK

T. Yatagai
Institute of Applied Physics, University of Tsukuba, Sakura, Ibaraki, Japan

S. Yokozeki
Department of Applied Physics, Osaka University, Suita, Osaka, Japan

OPTICS and LASERS in ENGINEERING

VOL. 9 1988

Editors

F. P. CHIANG

G. T. REID

ELSEVIER APPLIED SCIENCE

© 1988 Elsevier Applied Science Publishers Ltd

All rights reserved. No part of this publication may be reproduced, stored in a retrieval system, or transmitted in any form or by any means, electronic, mechanical, photocopying, recording, or otherwise, without the prior written permission of the publisher, Elsevier Applied Science Publishers Ltd, Crown House, Linton Road, Barking, Essex IG11 8JU, England.

Special regulations for readers in the USA. This journal has been registered with the Copyright Clearance Center, Inc. Consent is given for copying of articles for personal or internal use, or for the personal or internal use of specific clients. This consent is given on the condition that the copier pay through the Center the per-copy fee stated in the code on the first page of each article for copying beyond that permitted by Sections 107 or 108 of the US Copyright Law. The appropriate fee should be forwarded, quoting the code number at the end of this paragraph, to the Copyright Clearance Center, 21 Congress Street, Salem, MA 01970, USA. If no code appears in an article, the author has not given broad consent to copy and permission to copy must be obtained directly from the author. This consent does not extend to other kinds of copying, such as for general distribution, resale, advertising and promotion purposes, or for creating new collective works. Special written permission must be obtained from the publisher for such copying. 0143-8166/88/$03.50.

Special regulations for authors: Upon acceptance of an article by the journal, the author(s) will be asked to transfer copyright of the article to the publisher. The transfer will ensure the widest possible dissemination of information.

Note. No responsibility is assumed by the Publisher for any injury and/or damage to persons or property as a matter of products liability, negligence or otherwise, or from any use or operation of any methods, products, instructions or ideas contained in the material herein.

Although all advertising material is expected to conform to ethical standards, inclusion in this publication does not constitute a guarantee or endorsement of the quality or value of such product or of the claims made of it by its manufacturer.

Printed in Northern Ireland at The Universities Press (Belfast) Ltd

Optics and Lasers in Engineering **9** (1988) 1–12

Effects of Plasma on CO_2 Laser Cutting Quality

B. S. Yilbaş & Z. Yilbaş

Erciyes Üniversitesi, Mühendislik Fakültesi, Kayseri, Turkey

(Received 24 February 1987; accepted 28 July 1987)

ABSTRACT

In CO_2 laser cutting, the measurement of plasma size and transmittance is necessary since the plasma appearing on the surface of the workpiece absorbs a fraction of the incident energy and acts as a heat source, enhancing the cutting process. Consequently, when the plasma size increases, the energy distributed across the plasma becomes lower and the energy losses due to heat transfer increase. This increases the heat-affected zone and reduces the cutting quality.

In the present study, CO_2 laser cutting of sheets of mild steel and titanium is examined while varying the cutting speed. Oxygen (as a reactive gas) and an argon/oxygen mixture are introduced through a nozzle in the cutting section. In order to examine the effect of the plasma on the cutting performance and quality, O_2 and gas mixture pressures are varied and the absorption of the He–Ne beam passing through the plasma in the direction normal to the CO_2 beam axis measured. It is found that the cutting quality improves at a particular O_2 pressure for the mild steel workpiece. The absorption of plasma increases as the cutting speed reduces.

INTRODUCTION

To overcome reflection during CO_2 laser cutting of many engineering materials two suggestions have been made:[1] (1) use of oxygen or an oxygen/inert gas mixture in the cutting section; (2) surface coating of the workpiece. The surface coating is defined as any material which is

Optics and Lasers in Engineering 0143-8166/88/$03·50 © 1988 Elsevier Applied Science Publishers Ltd, England. Printed in Northern Ireland

placed on the surface of the workpiece to absorb the incident CO_2 laser radiation energy and transmit it by conduction to the workpiece. However, surface coating creates secondary costs and entails the extra work of removal from the surface after cutting.

Alternatively, two different cutting techniques have been developed with the introduction of a gas in the cutting section.[2] (1) In laser fusion cutting the material is melted by the radiation energy of the laser and the melt is blown by a gas introduced from a nozzle. In this case shielding gas is required for combustible materials. (2) The material may be eroded by vaporisation, i.e. oxygen is used in the cutting section. In laser oxygen cutting, material is heated to ignition temperature by the focused laser beam. Consequently, a high temperature oxidation, exothermic reaction takes place during the cutting. This reaction provides extra energy in the cutting section. The oxygen provides: (a) increased absorption of incident laser energy by the workpiece; (b) considerable additional energy through the exothermic reaction, increasing the cutting process; (c) cleaning of molten metal oxide from the cutting section; and (d) cooling and protection of the focusing lens from liquid and vapour emission.

The laser cutting process is reported[3] to fill the gap left by conventional thermal cutting processes in the thickness range up to 5 mm. All types of metals and non-metallic materials can be cut. For cutting high alloy steels or aluminium of 150 mm thickness, plasma arc cutting is an alternative technique that must be considered.[3] It has also been reported[4] that the CO_2 laser can be used to advantage for processing small and medium sized production batches of less than 1000 units. Laser cutting has been found to be faster, in some cases, than sawing, milling or shearing, e.g. in the manufacture of air conditioning equipment.

In the present study, CO_2 laser cutting of 0·8-mm thick sheets of mild steel and titanium is examined while varying the cutting speed. O_2 (as reactive gas) and $Ar–O_2$ gas mixture are introduced through a nozzle in the cutting section. It must be noted that selection of different workpiece materials is based on their range of thermal properties. Since the milling table is controlled by a computer, the cutting speed is varied between 0·1 and 0·2 in s^{-1} which was the maximum obtainable. In laser cutting, when the plasma size increases, the energy distributed across the plasma becomes lower and the energy losses due to heat transfer increase. This increases the heat-affected zone and reduces the cutting quality. In order to examine the effect of plasma on the cutting performance and quality, the oxygen gas pressure is varied and the absorption of the He–Ne beam passing through the plasma in the

direction normal to the CO_2 beam axis is measured for titanium workpieces. Finally, the quality of the cut is assessed and the properties of the cut surface discussed.

METHODS

Experimental apparatus

The experimental set-up is shown in Fig. 1. A CO_2 laser giving a mean output power of 350 W (cw) was used. The laser beam was emitted horizontally and deflected vertically downwards towards the workpiece by means of a 45° gold-plated stainless steel mirror, which was angularly adjustable. At the end of the laser assembly a potassium chloride lens with nominal focal length of 4 in. was fixed in a lens holder which could move in the vertical direction so that the different focus settings could be obtained. In order to measure the instantaneous laser output power a calorimeter was placed between the semi-reflecting mirror and the 45° deflector.

Oxygen was introduced coaxially with the laser beam through a nozzle of about 1 mm diameter at the workpiece surface. The nozzle had no aperturing effect on the laser beam which at that point was less than 1 mm.

The milling table was controlled by a computer. The speed of the table was variable and the maximum speed obtainable either in the x

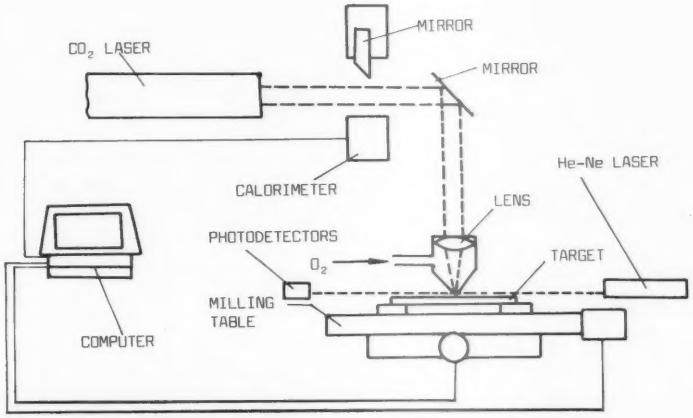

Fig. 1. Experimental apparatus.

or y direction was limited to 0·25 in. s^{-1}. This speed level was sufficient for the present requirements.

To measure the plasma absorption as described earlier, a He–Ne laser delivering 2 mW output power was employed with its beam passing through the plasma, parallel to the workpiece surface and orthogonal to the CO_2 laser beam axis.

Two BP × 65 photodiodes[5] with fast responses were positioned 5 mm apart and 30 cm away from the irradiated surface. This allowed the photodiodes to see the same spatial locations in the plasma. This was necessary because the plasma was transient in nature.

Calibration of focus settings

The measurement of the relative position of the focal plane of the focusing lens was also important. For this a 0·1-mm-thick thermal sensitive paper was placed onto the specimen plate. This assembly was then traversed under the laser beam. In order to avoid the burning of the paper, the inert gas (argon) was discharged at a pressure of 30 psi through a nozzle onto the paper. Consequently, the laser produced a cut on the paper. This procedure was repeated for different focal settings. The cuts were examined under the microscope to determine the thinnest cut. This was held to be the focal plane since the beam width was narrowest at this position. The minimum cut width measured was 80 μm in the present case. Note that the laser output power was lowered to 60 W during the measurement.

The cut width was also determined theoretically using an Airy Disc formula:

$$r = (1{\cdot}22\lambda\,\mathrm{FN})/n$$

where FN = focal length/diameter of lens, n is the refractive index of the lens and λ is the wavelength of the laser beam. After substituting appropriate values into the Airy Disc formula, the cut width was calculated to be 72 μm (this agreed with the Bakewell[6] results obtained from the diffraction integral). This is in good agreement with the experimental result.

The photodiode (BP × 65) outputs were recorded simultaneously using a storage oscilloscope during the cutting.

Evaluation of cut quality

The laser cutting performance requires close examination of the surface properties of the cut. The cut quality may be successfully evaluated in

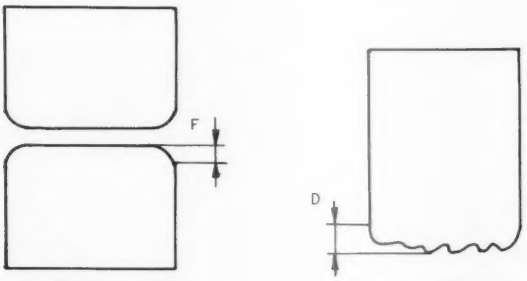

Fig. 2. Measurement of unevenness (F) and clinging dross (D).

terms of clinging dross, flatness and surface hardness (Fig. 2), provided that the assessment for the cut quality is based on the international standards for thermal cuts.[7] Height of clinging dross was measured with a micrometer, flatness of the cut was measured with a reading microscope and surface hardness was measured with microhardness measuring equipment (Zeiss).

Measurement of transmittance

The He–Ne laser beam first passed through the section under examination until it reached one of the photodiodes. This resulted in a difference in photodetection output. In order to observe the absorption during CO_2 laser cutting, the photodiode outputs were initially set to coincide. Once the cutting started, plasma developed and both photodiodes gave responses, one due to thermal radiation from the plasma and the other due to thermal radiation and the He–Ne laser beam. The plasma absorbed and blocked some fraction of the He–Ne beam, resulting in a shift in direction opposite to the gain of the photodetector outputs. This appeared as a gap between two signals on the oscilloscope screen, as shown in Fig. 3. Since the initial difference due to the He–Ne laser beam was known, the transmittance (I/I_0) could be measured. Each experiment was repeated twice, and the results obtained were found to be in agreement. The deviation of output signals of the photodetector due to thermal radiation was also taken into account. This was achieved by switching off the He–Ne laser before firing the CO_2 laser. The outputs are given in Fig. 3 when the He–Ne laser is on and the CO_2 laser is off.

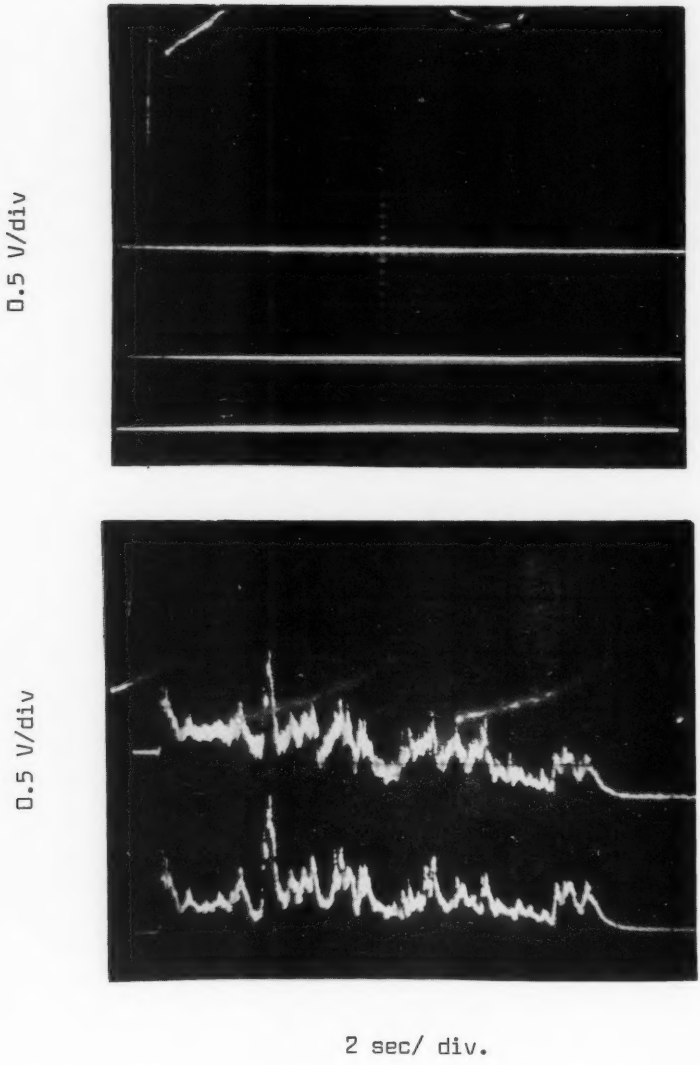

Fig. 3. Photodiode outputs. (a) He–Ne laser on and CO_2 laser off. (b) He–Ne and CO_2 lasers both on.

DISCUSSION

When the laser beam interacts with the workpiece surface, thermal energy originates in the region of the workpiece surface and is conducted into the material from the point of beam impingement. This is true up to a critical energy density of the beam, as the process of cutting falls into two phases. Firstly, the laser beam must break through the metal surface and secondly a deep penetration keyhole must be formed. Failure in the first phase was the main reason for not obtaining the cutting. On the other hand, since the CO_2 laser beam is infrared radiation, it is easily reflected by the bright molten metal puddles or by the workpiece surface. As a consequence of this a fraction of the radiated energy is lost. This would lead to surface damage rather than cutting. To achieve cutting a surface plasma must be generated and the plasma size may be increased by the use of O_2 in the cutting section. However, the plasma generated on the workpiece surface becomes an intermediate medium between the workpiece and the incident laser beam, absorbing the incident energy. Alternatively, plasma acts as a heat source affecting the cutting process.

The variation of transmittance with time using various mixtures of Ar/O_2 is given in Fig. 4 for 0·8-mm-thick titanium workpieces. It can be

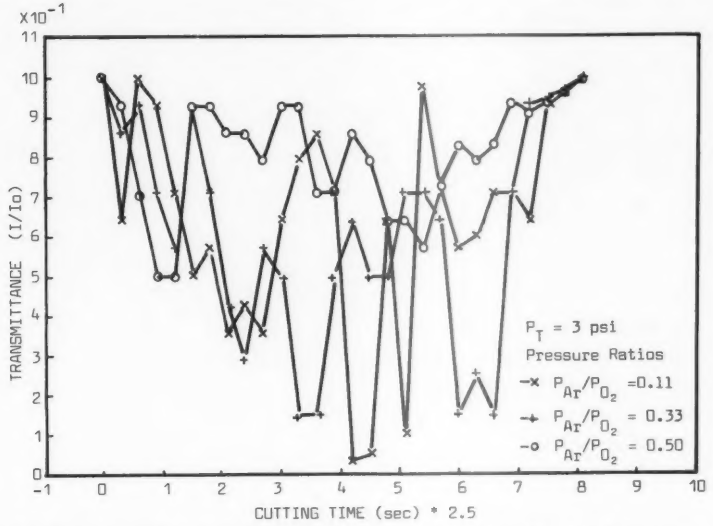

Fig. 4. Transmittance test results for titanium workpiece (P_T = total pressure of mixture).

TABLE 1
Clinging Dross (D) and Unevenness (F) Measurements for Titatium Workpiece (Cutting Speed = 0·25 in. s^{-1})

	O_2 pressure (psi)				*Ar/O_2 pressure ratio*[a]			
	Atm.	*1*	*2*	*3*	*3*	*1*	*0·33*	*0·11*
D (mm)	4·5	4·6	4·8	4·8	—	3·8	3·6	4
F (mm)	0·26	0·26	0·26	0·26	—	0·25	0·2	0·24

[a] Total pressure of mixture = 3 psi.

seen that the transmittance oscillates considerably with time. This may be due to the transient characteristics of the titanium plasma in which the charged and neutral particles are very mobile.[8] The transmittance decreases to 0·05 when the partial pressure of O_2 is increased to 2·7 psi in the gas mixture. This may be explained in terms of the properties of the workpiece material: titanium has high thermal diffusivity, low absorption coefficient and high oxidisation potential.[9] Consequently, when the partial pressure of O_2 in the gas mixture is increased, the high temperature oxidation increases resulting in excess energy, increasing the rate of melting and evaporation. This also increases the plasma size and reduces the transmittance. Alternatively, when Ar pressure in the gas mixture is increased, the transmittance increases and the cutting quality improves as evident from Table 1. However, when Ar pressure in the mixture is increased further while keeping the mixture pressure constant, cutting ceases. This happens at 2·25 psi Ar pressure when the mixture pressure is kept at 3 psi.

In Fig. 5, the variations of transmittance with time for a titanium workpiece are given for a cutting speed of 0·25 in. s^{-1} and at different O_2 pressures. The transmittance decreases to 0·03 as the pressure of O_2 increases. In addition, the size of the kerf increases, resulting in poor cutting quality as the pressure of O_2 increases. This may be due to the plasma characteristics and the thermal properties of titanium as described earlier.

In Fig. 6 the microhardness test results are given for a titanium workpiece. The hardness decreases at the near edge of the kerf and increases as the distance from the kerf edge increases. The hardness reaches its maximum after a distance of 4 mm. This may be due to the fact that in this particular case, the size of the plasma is large and the plasma acts as a heat source for the workpiece material, resulting in a large heat-affected zone.

It is evident from Table 1 that a high cutting quality is obtained at an Ar/O_2 pressure ratio of 0·33 for a titanium workpiece. In general, the

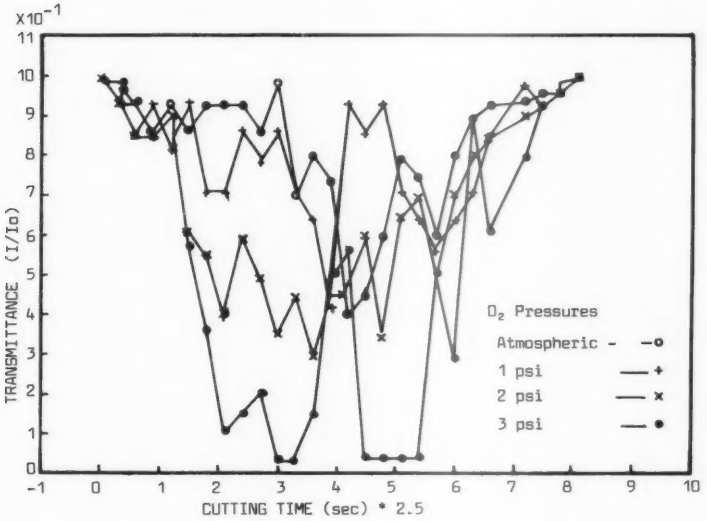

Fig. 5. Transmittance test results for titanium workpiece.

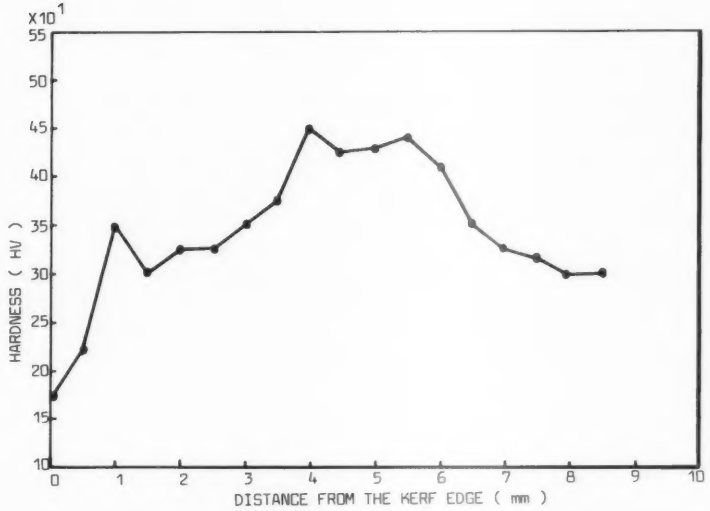

Fig. 6. Hardness test results for titanium workpiece.

TABLE 2
Width of Heat-affected Zone (mm) for Titanium (Cutting Speed = 0·25 in s^{-1})

Distance along cut (mm)	*O_2 pressure (psi)*				*Ar/O_2 pressure ratio*[a]			
	Atm.	*1*	*2*	*3*	*3*	*1*	*0·33*	*0·11*
0	7	7·7	6	7	—	4·5	5·5	8·25
10	8	8	6·5	8	—	4·5	5·3	11
20	8·5	8	5	9	—	6·2	6·2	8
30	7·5	7·5	8	8	—	6·3	6·3	1·8
40	7	8·5	4	9	—	6·3	6·2	2·8
50	7	9·5	6·5	9·2	—	6·2	6·2	4·5
60	7	8·5	3	9	—	6·3	6·1	6

[a] Total pressure of mixture = 3 psi.

use of O_2 in the cutting section lowers the cutting quality markedly for a titanium workpiece. This may be due to the effect of plasma and the material properties as mentioned earlier.

In Table 2 the width of the heat-affected zone produced at various Ar/O_2 pressure ratios and O_2 pressures is given for a titanium workpiece. The width of the heat-affected zone corresponding to Ar/O_2 gas cutting is usually lower than that corresponding to O_2 cutting. However, the heat-affected zone for a titanium workpiece resulting from both Ar/O_2 and O_2 gas cutting is larger than that obtained in the case of mild steel.

The width of the heat-affected zone for the mild steel workpiece resulting at 0·1 in. s^{-1} cutting speed with the distance along the cut is given in Table 3 for different O_2 pressures. In general, the heat-affected zone is very small indeed, i.e. of the order of 1·25 mm. The heat-affected zone obtained at 4 and 5 psi O_2 pressures varies considerably with the distance. This may be due to the plasma effect. This occurs in such a way that at some cutting time the plasma size increases for low cutting speed and high O_2 pressures. Since the plasma acts as a heat source, a wide heat-affected zone is obtained in this case. This is supported by the transmittance test results, as discussed earlier. However, the heat-affected zone corresponding to the cutting speed of 0·2 in. s^{-1} is lower than that obtained at 0·1 in. s^{-1} cutting speed, and is of the order of 0·9 mm. This may again be due to the plasma effect as described earlier. This proves that the effect of the plasma on the cutting process is less significant in the case of the 0·2 in. s^{-1} cutting speed, as suggested by previous work.[10]

TABLE 3
Width of Heat-affected Zone (mm) for Mild Steel at Two Cutting Speeds

Distance along cut (mm)	*Cutting speed 0·1 in. s^{-1}*				*Cutting speed 0·2 in. s^{-1}*			
	O_2 pressure (psi)				*O_2 pressure (psi)*			
	2	*3*	*4*	*5*	*2*	*3*	*4*	*5*
10	1	1·25	0·8	1·25	0·8	0·7	0·7	0·9
20	1·25	1	0·8	1	0·8	0·8	0·8	0·9
30	1·5	1·25	1	1	0·8	0·7	0·7	1·2
40	4·5	1	1·25	1	0·8	0·7	0·9	1
50	4	1	1	1·2	0·8	0·7	0·7	0·9
60	1·5	1·5	1·1	1·15	0·8	0·7	0·7	0·9

TABLE 4
Clinging Dross (D) and Unevenness (F) Measurements for Mild Steel at Two Cutting Speeds

O_2 pressure (psi)	*Cutting speed 0·1 in. s^{-1}*		*Cutting speed 0·2 in. s^{-1}*	
	D (mm)	*F (mm)*	*D (mm)*	*F (mm)*
2	0·4	0·15	0·1	0·2
3	0·25	0·1	0·15	0·08
4	0·3	0·15	0·2	0·1
5	0·3	0·1	0·15	0·1

Table 4 shows the measured values of the clinging dross and unevenness corresponding to 0·1 and 0·2 in. s^{-1} cutting speeds for a mild steel workpiece. It can be seen that D and F have values of the order of 0·35 and 0·15 mm, respectively, in the case of 0·1 in. s^{-1} cutting speed. However, D decreases to about 0·2 mm in the case of 0·2 in. s^{-1} cutting speed. This may be due to the effect of O_2 pressure at low cutting speeds as described earlier. When the results given in Table 4 are compared to the international standards,[7] it is found that they are very high, indicating high quality cuts.

CONCLUSIONS

The transmittance is very low in the case of the titanium workpiece. This may indicate that the effect of plasma on the cutting process is significant.

A large heat-affected zone is obtained for titanium workpieces at all gas mixture pressure ratios and O_2 pressures. This may also indicate the significant effect of plasma on the cutting process.

The quality of cut for titanium workpieces improves if the Ar/O_2 mixture is used instead of O_2 alone in the cutting section.

The heat-affected zone produced in a mild steel workpiece is large and is of the order of 0·8 mm at a cutting speed of 0·2 in. s^{-1}.

A high quality of cut is obtained at a cutting speed of 0·2 in. s^{-1} and an O_2 pressure of 3 psi for a mild steel workpiece.

REFERENCES

1. Schaffer, G., Laser cutting replaces blanking, *Source Book of Laser Applications,* ASM publication, 1981, pp. 30–40.
2. Hoffman, M., The laser as an industrial cutting tool, *Metal Const.,* Jan. (1979) 88–9.
3. Cooper C., An investigation into parameters effecting the cutting efficiency of a cw CO laser, M.Sc. thesis, Mech. Eng. Dept., University of Birmingham, 1973.
4. Bolin, S., Laser welding, cutting and drilling Part I, *Source Book of laser Applications,* ASM publication, 1981, pp. 30–34.
5. R. S. Components, R. S. Components library, Data sheet no. 2135, Dec., 1981.
6. Bakewell, B. A., Performance of pulsed laser system in relation to machining mechanisms, Ph.D. thesis, Mech. Eng. Dept., University of Birmingham, 1973.
7. International Standards. West Germany standard no. DIN2310.
8. Yilbaş, B. S., Heat transfer mechanisms initiating the laser drilling of metals, Ph.D. thesis, Mech. Eng. Dept., University of Birmingham, 1981.
9. Harrison, R. D., *Advanced Science Book of Data,* Longman, London, 1984.
10. Yilbaş, B. S., Study into effect of plasma during CO_2 laser cutting of metal sheets, Research report, Mech. Eng. Dept., University of Birmingham, 1986.

Optics and Lasers in Engineering **9** (1988) 13–22

Use of a CO_2 Laser for Thermal Effect Simulation on Sintered Carbide Inserts

O. De Pascale, C. Esposito

Centro Laser, Via F. De Blasio, 1, 70123 Bari, Italy

M. Lepore

Dip. Fisica, Univ. Bari, Via Amendola, 173, 70123 Bari, Italy

S. Lo Casto & G. Passannanti

Dip. Tecnologia e Produzione Meccanica, Univ. Palermo, Viale delle Scienze, 90128 Palermo, Italy

(Received 24 August 1986; revised version received 12 May 1987; accepted 25 August 1987)

ABSTRACT

In order to study the thermal behaviour of sintered carbide inserts during interrupted cutting, thermal cycles have been carried out by using a CO_2 high-power laser with different conditions to simulate the actual cutting stress.

It has been pointed out that the use of a laser is adequate for this purpose and that, even should the thermal fractures themselves not cause the collapse of the inserts, the thermal actions alone will be responsible for the growth of microfractures which weight heavily in predicting tool life.

INTRODUCTION

For several years research has been carried out on the life of edges of inserts of sintered carbides in interrupted cutting.

From studies carried out it has been affirmed that the end of life of the inserts is caused by a mechanical phenomenon; the rapid variation of stress on the rake face of the insert both at the engagement and disengagement of the workpiece,[1–4] as well as a phenomenon of thermal

Optics and Lasers in Engineering 0143-8166/88/$03·50 © 1988 Elsevier Applied Science Publishers Ltd, England. Printed in Northern Ireland

stress (heating during cutting and cooling during non cutting).[5] So as to clarify to what extent each of these factors contributes to the fracturing of the inserts and intervenes as necessary in the phase of practical application, these two phenomena must be studied separately.

It has been possible to isolate and study this mechanical phenomenon easily by having the insert undergo repeated impact up to breaking point by means of guillotine-like apparatus,[6] thus simulating the impact of the insert on the rotating workpiece. So as to simulate this thermal effect various methods were proposed; resistance heating,[7] furnace heating[8] and induction heating.[9]

However, these methods present drawbacks insofar as they do not permit a close control of the rate of heating and cooling and the thermal cycles with relatively high frequency which are encountered in milling operations. Furthermore, in certain cases, the methods studied do not cause the thermal gradient inside the insert which is created during the actual cutting operation and which is the cause of the phenomenon leading to the initial and continued cracking.

In order to isolate the thermal effect, it was thought that the use of a pulsed laser could offer a solution to the problem of heating the rake face over an area almost equal to the tool–workpiece contact zone, with pre-set temperature gradients similar to those observed during the actual cutting process. In fact, a laser beam has the advantage of a non-contact, fast and clean heating; on the other hand there are some drawbacks. For example, the surface temperature of the sample depends on the material absorption properties at the beam wavelengths and the absorption itself may vary both for different samples and, for the same one, during the experiment, owing to eventual surface modifications. In addition, the expected temperature build-up inside the surface normally causes an increase in the instantaneous temperature over the pre-set value, and the use of decreasing pulse energy is difficult.

All such problems can be overcome if a temperature sensor, connected in a fixed loop with the laser, is employed. In this way, one can enjoy all the advantages of using a laser in heating, and any thermal cycle can be obtained on the sample independently of the surface properties and of the heat stored in the samples.

In this paper, the device able to perform these heating cycles will be described and some preliminary results will be shown.

THE LASER DEVICE

For the experiments, a CO_2 slow axial flow laser (VALFIVRE LIS-500) with electronic discharge control was used. Such a laser may also be

driven from external devices simply by applying a positive low level input electrical signal in order to control the power in the range 20–500 watts. Response times of the beam power are less than one hundred microseconds.

The peak temperature to be applied to the samples varied from 800 to 1100 °C. At such temperatures, the blackbody emission in the near-infrared wavelength region is strong enough to be revealed, e.g. by a silicon photodiode, with the additional advantage of a fast response. Moreover, the intensity per unit area of the emitted radiation in the wavelength range of interest is a rapidly growing monotonic function of the temperature, so feedback operation is possible. However, a calibration with bodies at a known temperature was required after the collecting lens and photodiode were mounted inside a suitable case.

The equipment was designed to detect the temperature over a circular area with about 0·9 mm diameter, while the CO_2 laser beam was used defocused on a larger spot. In addition, the laser cavity was carefully aligned in order to obtain a low-order mode beam. In Fig. 1 the simplified experimental set-up is shown. In Figs 2 and 3 the system closed-loop response to two different waveforms (Figs 2(a) and 3(a)) applied to the temperature control input are shown. Figs 2(b) and 3(b) show the photodiode signal after the PD amplifier, while in Figs 2(c) and 3(c) the laser controlling voltages (at the output of the error amplifier) are reported.

Voltages shown in Figs 2(c) and 3(c) may be intended as roughly proportional to the beam power with a 100W div^{-1} approximate scale.

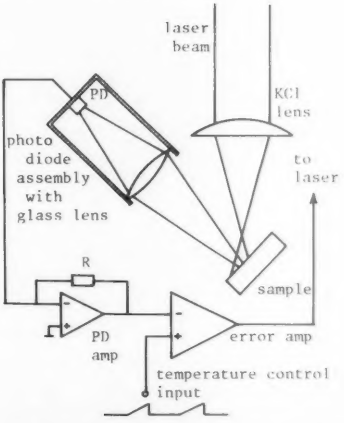

Fig. 1. Simplified experimental set-up.

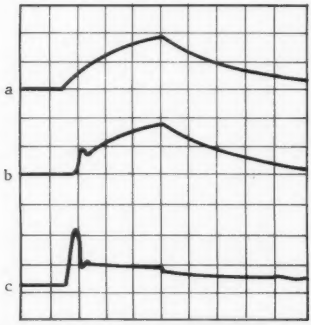

Fig. 2. Electric waveforms at three different points of the loop: (a) at the temperature control input (0·5 V vertical division^{-1}); (b) at the PD amp output (0·5 V vertical division^{-1}); (c) at the error amp output (1 V vertical division^{-1}). Timebase: 10 ms horizontal division.$^{-1}$

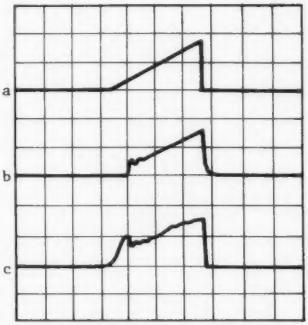

Fig. 3. Electric waveforms at three different points of the loop: (a) at the temperature control input (0·5 V vertical division^{-1}); (b) at the PD amp output (0·5 V vertical division^{-1}); (c) at the error amp output (1 V vertical division^{-1}). Timebase: 10 ms horizontal division.$^{-1}$

The conversion factor for the temperature (Figs 2(a), (b) and 3(a), (b)) requires some comment. Owing to the particular wavelength range chosen for detection (from 0·8 to 1 micrometer, obtained by placing a long pass optical filter in front of the photodiode), the photocurrent roughly doubles for a 100°C increase on the temperatures of interest. While ensuring a precise temperature recognition, this very approximate exponential dependence is thought to be responsible for both the delay and the overshoot spike in Figs 2(b) and 3(b). In an equivalent manner it can be said that the diode is almost 'blind' under 700 °C, hence both signals in Figs. 2(a) and 3(a) involve a temperature rise which is too fast for the system. It must also be said that the error amplifier speed had to be slowed by means of a pole compensation (time constant in the order of 10 ms), for stability purposes.

The peak temperature to be read in the figures corresponds to 1000 °C. As noticed before, 1000 °C correspond to about one half the 1100 °C signal height, and so on. As can be seen, there is a close matching between parts (a) and (b) of Figs 2 and 3. Moreover, Fig. 2 gives an example of a laser-sustained cooling, while in Fig. 3 the sample cooling is 'natural'. This latter waveform was used for the experiments, in order to simulate repeated tool–workpiece interactions, with natural cooling between one another.

TEST EXECUTION AND RESULT ANALYSIS

These tests carried out on inserts of sintered carbides SNGN 120408, grade P10, were performed by simulating the conditions for four different cutting operations similar to those utilized in preceding works,[10] as referred to in Table 1. For each of these tests ten different edges were employed. The inserts were fixed to a commercial tool holder so as to reproduce the conditions of dispersion of heat from the lower face of the insert and in this way bring about a temperature gradient inside the insert as close as possible to the actual conditions of cutting.

The tool holder was mounted on equipment that made it possible to register the position of the insert with relation to the laser beam.

At the beginning of each test it was observed that the power absorbed from the laser beam was at a maximum, insofar as the considerable absorption of heat by the cold mass of the insert was an obstacle to it immediately reaching the pre-set temperature. After a few seconds, however, the system reached a steady state and the power absorption was drastically reduced. Preliminary tests showed that the thermal stress alone (using the laser beam), though it brought about an obvious damaging, nonetheless did not cause a fracturing of the insert as was verified during cutting, except after prolonged treatment in heavy work conditions ($T > 1200\,°C$). As it was impossible to establish the average life of the inserts up to the fracture point for each heating operation during the tests, it would have been necessary to establish the maximum level of damage and to carry out thermal cycles so as to reach this level This would imply periodic interruption of the tests so as to verify the conditions of the edge with a resulting loss of the steady state reached. Consequently we decided to carry out the same number of thermal cycles on each of the edges and measure the level of damage reached on each one. So all the edges underwent 12 000 cycles. In Fig. 4 we can observe the aspect of the portion of the insert between the

TABLE 1

Simulated operation conditions	*Heating (ms)*	*Cooling (ms)*	*T (°C)*	*σ (Kg mm^{-2})*	*h (micron)*
1	30	70	900	89	—
2	33	38	900	95	6·0
3	21	68	1000	106	15·6
4	19	44	1000	110	21·4

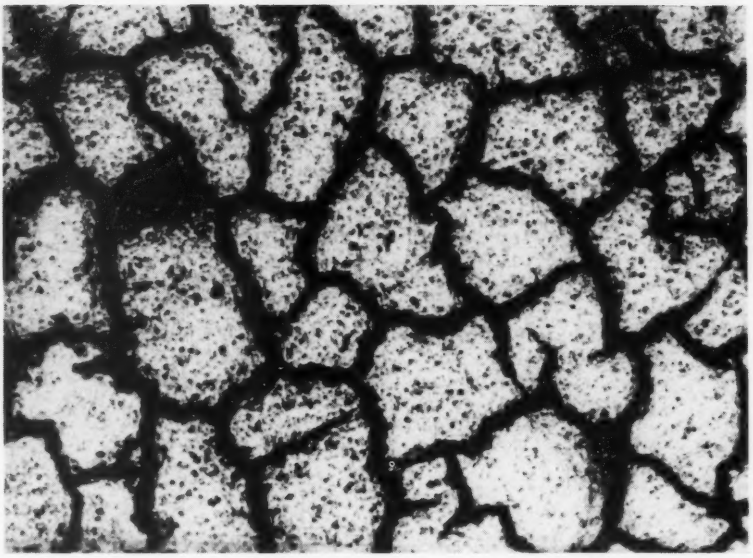

Fig. 4. Effects produced by thermal cycles on the rake face of an insert of sintered carbides.

area directly heated up by the laser beam and the edge of the insert. Its aspect is typical of 'dry mud' as already defined by other researchers.[11,12]

The level of damage to the insert can be quantified in various ways: by measuring the length and width of the fractures produced, and by measurement of both their depth and dimensions of the scales.

It would seem that the degree of damaging can be most accurately quantified by assessing the depth of the fracturing produced. But we must consider that the width of the fractures is inferior to their depth and as a consequence measuring with the profilometer (under these circumstances) is not possible.

If the inserts are exposed to an ultrasonic treatment for 30 min, we observe the detachment of certain scales. This can be justified as follows: during the cooling-off phase of the insert at a layer close to its surface, a particular temperature gradient, positive at its inside level, is established. We can suppose that the ensuing differentiated contractions of the scales, isolated by the fractures coming out of the external surface, tend to create a curving (Fig. 5).

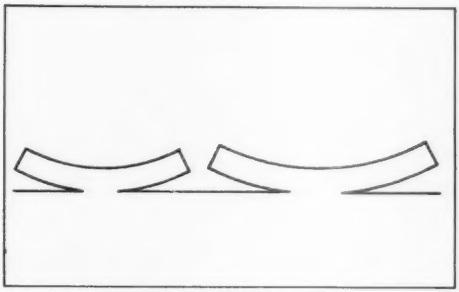

Fig. 5. Aspect of scales.

This causes the start of fractures which are orthogonal to the principal cracks, the former are all the more accentuated in relation to the depth of the latter. This cracking, which propagates itself because of the ultrasonic effect, brings about the detachment of a scale the width of which is equal to the depth reached by the fracture. In this manner we can use the profilometer to measure the depth of the fracture.

The detachment of scales did not come about, even where the application of ultrasonic equipment was effected over a longer period of time, for those inserts that had undergone even the lowest thermal cycles. Table 1 reports, in the last column, the average measurement of the depth of fractures under the four different simulated cutting operations.

In the second to last column of the same table, we have reported the values relative to the positive thermal stress that arises during the cooling-off phase of the insert, as calculated according to the method set out in a preceding work.[10] In particular, the stresses have been determined by making the hypothesis that the rake face of the tool coincide with the median plane ($y = 0$) of a slab twice as thick as the insert thickness. In this case, for temperature distributions symmetric with respect to this plane, it is[13]:

$$\sigma_x = \sigma_z = -\alpha E(\vartheta - \vartheta_m)/(1 - \nu)$$

where the temperature distribution has been determined using the relation[5]:

$$\frac{\vartheta(y, d) - \vartheta_a}{\Delta\vartheta - \vartheta_a} = 1 - \operatorname{erf}(y, a, t)$$

where:

$\alpha E/(1-\nu) = 3{\cdot}92$ M Pa °C^{-1},

$a = k\rho/c$ = thermal diffusivity = $0{\cdot}25$ cm^2 s^{-1},

ϑ_a = room temperature,

t = time,

$\Delta\vartheta$ = temperature step for a time rise equal to (heating time)/20 or (cooling time)/40, according to the phase considered.

Figure 6 reports fracture depth versus thermal stress. The equation of the curve interpolating experimental points is:

$$h = K\sigma^{8{\cdot}68} \tag{1}$$

where:

h = depth of fracture

σ = superficial thermal stress

K = constant depending on the tool material and the number of cycles.

For the experimental conditions used, the value of K is $4{\cdot}0 \times 10^{-17}$. The equation obtained is similar to that reported by other researchers[14]

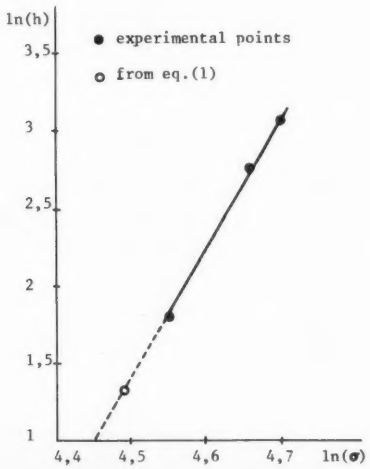

Fig. 6. Fracture depth versus thermal stress.

on fatigue crack growth rate, particularly the exponent of σ which is equal to that determined for the range of the stress intensity factor.

CONCLUSION

The thermal actions alone are responsible for the propagation of microfractures which we suppose to exist in sintered materials. Even if the thermal fractures themselves do not cause the collapse of the insert, they certainly do affect its reliability; in fact the tool life is in an inverted ratio to the depth of the fracture itself.

In the same mechanical conditions, the life of inserts will not be constant but strongly affected by thermal conditions which weigh heavily in predicting tool life.

Use of high-power lasers appears to be an adequate method of simulating the thermal conditions for interrupted cutting. We can therefore forecast that the test method described, opportunely reviewed, might be used for the qualification of cutting inserts, constructed with new materials designed principally for high cutting speed, for which the thermal stress conditions have even greater importance.

REFERENCES

1. Loladze, T. N., Nature of brittle failure of cutting tool, *Annals of the CIRP*, **24** (1) (1975) 13–16.
2. Pekelharing, A. J., The exit failure of cemented carbide face milling cutters—part I: fundamentals and phenomena, *Annals of the CIRP*, **33** (1) (1984) 47–50.
3. Lo Casto, S., Passannanti, G. & Piacentini, M., Influenza degli angoli di ingresso ed uscita sulla vita dei taglienti nel taglio interrotto, *La Meccanica Italiana*, **189** (Aprile 1985) 37–41.
4. Chandrasekaran, H., Tool fracture model for periferal milling, *10th NAMRC*, (1982) 15–20.
5. Uehara, K., Fundamental approach to the thermal crack of cement cutting tools, *Annals of the CIRP*, **30** (1) (1981) 47–51.
6. Hirao, M., Murata, R., Kasuya, U. & Takeyama, H., Evaluation of cutting tool toughness through non-cutting test, *Annals of the CIRP*, **28** (1) (1979) 29–32.
7. Okushima, K. & Hoshi, T. Thermal crack in the carbide face-milling cutter, *Bull. of JSME*, **6** (1963) 317–26.
8. Tumanov, V. I., Goldberg, Z. A., Chernyshev, V. V. & Pavlova, Z. I., Thermal shock resistance of tungsten carbide–cobalt alloys, *Poroshk. Metallurgiya*, (Oct. 1966) 71–7.

9. Chandrasekaran, H., Thermal fatigue studies on tool carbides and its relevance to milling cutters, *Annals of the CIRP*, **34** (1) (1985) 125–8.
10. Lo Casto, S., Passannanti, A. & Passannanti, G., Influenza dei cicli termici sulla vita delle placchette in carburi sinterizzati, *La Meccanica Italiana*, **187**, (Jan./Feb. 1985) 55–61.
11. Cantoro, G., Lo Casto, Lo S. & Tarantino, S., Relationship between anodic surface crack state and radiation fall off in X-ray tubes, Accademia delle Scienze Lettere ed Arti di Palermo (April 1972).
12. Cantoro, G., Lo Casto, S. & Tarantino, S., New experimental apparatus and measurement techniques of radiation fall off in X-ray tubes, Accademia delle Scienze Lettere ed Arti di Palermo (April 1972).
13. Timoshenko, S. & Goodier, N., *Theory of Elasticity*, McGraw-Hill, New York, 1951.
14. Shibasaka, T., Hasimoto, H., Ueda, K. & Iwata, K., Analysis of brittle failure of cutting tools based on fracture mechanics, *Annals of the CIRP*, **32** (1) (1983) 37–41.

Optics and Lasers in Engineering **9** (1988) 23–34

The Preheating Temperature Parameter for Deep Penetration Welding With High Energy Focused Beams

R. Peretz

Laser-Kombinations-Systeme, Austrasse 29, 7315 Weilheim/Teck, FRG

(Received 31 August 1987; accepted 23 October 1987)

ABSTRACT

The effects of workpiece preheating at steady state deep penetration welding with high energy focused beams upon weld cross-section width and depth are investigated theoretically.

Parameter correlations, with special attention focused on the preheating of the workpiece are presented as analytic expressions and visualized in a nomograph. Preheating leads to weld width and depth increase. The theoretical correlations are in qualitative agreement with experimental results reported in the literature.

NOTATION

a	Thermal diffusivity ($m^2 s^{-1}$)
b	Weld width (m)
c_p	Specific heat ($J kg^{-1} K^{-1}$)
ETE	Energy transfer efficiency (−, %)
H_0	$= (2/\pi)K_0$, K_0 being the modified Bessel function of second kind and order zero
L	Melting heat ($J kg^{-1}$)
P	Power (W)
q_z	Local line source power (Wm^{-1})
r	Radius (m)
T	Temperature (K, °C)
t	Weld depth (m)
v	Welding speed (ms^{-1})
x	Coordinate (in the workpiece translation direction) (m)

Optics and Lasers in Engineering 0143-8166/88/$03·50 © 1988 Elsevier Applied Science Publishers Ltd, England. Printed in Northern Ireland

y Coordinate, half width of molten pool (subscript M) (m)
z Coordinate in the beam direction (m)
λ Thermal conductivity ($\mathrm{Wm^{-1}\,K^{-1}}$)

Dimensionless groups

K Ratio of material vaporization to melting temperature

$$K = T_V/T_M (T_V,\ T_M \text{ in } °C)$$

R Preheating parameter

$$R = T_\infty/T_M (T_\infty,\ T_M \text{ in } °C)$$

Ph Phase change number

$$Ph = L/c_{p,s}(T_M - T_\infty)$$
$$Ph_o = L/c_{p,s}T_M \qquad (T_M \text{ in } °C)$$

θ_V Vaporization temperature parameter

$$\theta_V = (T_V - T_M)/(T_M - T_\infty)$$

p_z Local power into workpiece (in the layer $[z,\ z + \mathrm{d}z]$)

$$p_z = q_z/\lambda_s(T_M - T_\infty)$$

N Global power into workpiece

$$N = t^{-1}\int_o^t p_z\,\mathrm{d}z = P_{KH}/\lambda_s(T_M - T_\infty)t$$

$Y_{z,M}$ Weld width (when subscript is not V)

$$Y_{z,M} = vb_z/a_s$$

Y_V Capillary radius

$$Y_V = 4(vr_V/2a_s)$$

η Dimensionless y coordinate

$$\eta = vy/2a_s$$

Subscripts

A Absorption
B Beam
$1/e^2$ Corresponding to the $1/e^2$-points of the gaussian beam intensity distribution
KH Keyhole
L Liquid
M Melting
o For $T_\infty = 0\,°C$ (no preheating)
P Pole

s Solid
V Vaporization
z At depth z (local value)
∞ In the workpiece, far from the beam impact region

Superscripts

$( )^-$ At melting isotherm intersection with the coordinate axis, negative location. $y_{\bar{M}}$ means the point on $y(x)|_{T=T_M}$ with $x=0$ and $y<0$.
$( )^+$ As $-$, but positive location
$(\bar{})$ At $z=0$ (top surface of the workpiece)
$( )'$ Part corresponding to solid phase
$( )''$ Into workpiece, taking phase change contribution into account.

INTRODUCTION

By improving the line source model[1,2] for workpiece temperature distribution with respect to resolidified weld cross-section profile[3] and melting latent heat effects,[4] analytic expressions which correlate the processing parameters and material thermophysical properties for deep penetration welding with high energy focused beams were derived in Ref. 5.

Based on the results mentioned above, an evaluation of preheating effects upon the resolidified weld cross-section geometry at steady state d.p.w. with focused beams becomes possible.

THE POWER INTO WORKPIECE AT DEEP PENETRATION WELDING

On the top surface of the workpiece, the 'key' (a laserbeam of power P_B and radius $\bar{r}_B$) enters the 'keyhole' (the capillary opening).

The efficiency of power transfer may be described by the following relationship:

$$P_{KH} = ETE_A \,.\, ETE_{KH} \,.\, P_B \tag{1}$$

where:

P_{KH} = power into workpiece via keyhole
ETE_A = absorption efficiency
ETE_{KH} = 'aperture' efficiency

At steady state processing, the absorption efficiency ETE_A is given by

the reflective properties of the melted material; it eventually depends also upon plasma clouding effects in the beam way to the workpiece. It is essential to notice that ETE_A does not depend on preheating temperature, because the vicinity of the beam-workpiece interaction region is already in melted condition. Preheating influences the value of the absorption efficiency only in unsteady processing (e.g. starting welding). The other factor which diminishes the power transferred in depth into workpiece is ETE_{KH}, the aperture efficiency.

The aperture efficiency is a highly sensitive function of the ratio of capillary radius (aperture radius) on the top surface of the workpiece to the beam radius at the same location (see Fig. 1, after Ref. 6).

If for example the capillary radius on the top surface of the workpiece $\bar{r}_V$ (superscript '$^-$' is used for the identification of this sheet) equals the $1/e^2$-points radius of the gaussian beam, only 86·5% of the nonreflected beam power penetrates the keyhole, the remaining 13·5% is blocked (lost) in the upper sheet.

In a more undesirable case, if $\bar{r}_V$ equals for example the $1/e$-points radius of the beam, only 63·2% of the nonreflected beam power gets into workpiece via the capillary walls, and 36·8% is blocked in the upper sheet, leading there to a distortion of the temperature distribution and to disproportional weld width increase in the top sheets of the workpiece ('weld head') to the prejudice of deep penetration.

If the processing parameters (workpiece velocity, beam power and

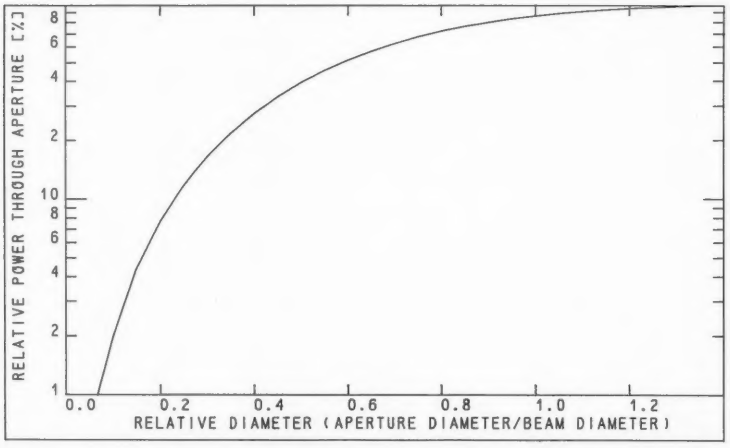

Fig. 1. Keyhole power for gaussian laser-beam welding (value 1.0 on the abscissa corresponds to the $1/e^2$-points radius).

focusing, preheating) are varied within adequate ranges, so as to always satisfy the condition (2), the aperture efficiency saturates in the vicinity of 95% (see Fig. 1) and may be considered a constant. The beam power is used herewith at its best from the point of view of deep penetration.

$$\bar{r}_V \geq 1{\cdot}2\bar{r}_{1/e^2} \tag{2}$$

We believe that at low power values (where most likely the condition (2) is not satisfied), preheating leads to an increase of the aperture efficiency, by $\bar{r}_V$ increase. This can be a reason for deep penetration improvement by workpiece preheating at low processing power values.

If, on the contrary, the processing parameters are within ranges so as to keep eqn (2) satisfied, preheating does not affect the ETE_{KH}-value any more, and making use of $\bar{r}_V = 1{\cdot}2\bar{r}_{1/e^2}$ gives good accuracy in the analytical treatment of the problem.

Analysis will now be made of the effects of preheating assuming condition (2) is satisfied or ETE_{KH} is known and invariant with preheating temperature.

THE CAPILLARY RADIUS ON THE TOP SURFACE OF THE WORKPIECE

The temperature distribution in the sheet $[z, z + dz]$ of the molten region of the workpiece which surrounds the capillary during processing is given, according to Ref. 4, by the equation

$$T_{L,z}(x, y) - T_{P,z} = (q''_z/4\lambda_L) \cdot \exp(vx/2a_s) H_0(v\sqrt{x^2 + y^2}/2a_s) \tag{3}$$

for $0 \leq z \leq t$ ($z = 0$ on the top workpiece surface, t is the weld depth) and

$$T_M \leq T_{L,z}(x, y) \leq T_V$$

T_L, T_P, q'' are functions also of z-location inside the workpiece (see Refs 3 and 5). Equation (3) is applicable for the top surface of the workpiece. Let us make use of the following boundary condition:

$$\bar{T}(x = 0, y_V^{\pm} = \bar{r}_V, z = 0) = T_V \tag{4}$$

Equation (4) makes the slightly egg-shaped isotherm $\bar{y}(x)\big|_{\bar{T}=T_V}$ of the temperature distribution in eqn (3) to match a circle $r = \sqrt{x^2 + y^2} = \bar{r}_V\big|_{\bar{T}=T_V}$ at $\bar{y} = \bar{y}_V^{\pm}$ (the circle corresponds to the rotational symmetry of the gaussian beam intensity distribution).

The following mathematical expression for the capillary radius on the

top surface of the workpiece could be obtained (see its derivation in the Appendix):

$$H_0(\bar{Y}_V/4) = \frac{1}{0{\cdot}5 + 0{\cdot}475\bar{Y}_M} + \frac{(\lambda_L/\lambda_s)(K-1)}{1 - R + 0{\cdot}4175 Ph_o \bar{Y}_M} \tag{5}$$

where $\bar{Y}_V = 4\bar{\eta}_V = 4(v\bar{r}_V/2a_s)$ = dimensionless capillary radius on the top surface of the workpiece, $\bar{Y}_M = 4\bar{\eta}_M = v\bar{b}/a_s$ = dimensionless weld width on the top surface of the workpiece, Ph_o = preheating temperature independent phase change number (corresponding to $T_\infty = 0\,°C$), $K = T_V/T_M$ = Ratio of material vaporization temperature, to melting temperature (T_V, T_M in °C) and $R = T_\infty/T_M$ = preheating parameter (T_∞ and T_M in °C). Equation (4) is identical with eqn (A16) of the Appendix.

THE NOMOGRAPH FOR DETERMINING THE EFFECTS OF WORKPIECE PREHEATING UPON WELD GEOMETRY

For a given material (known values of the thermophysical properties λ_L, λ_s, K, Ph_o etc.) the function $\bar{Y}_V(\bar{Y}_M)$ can be computed from eqn (5) and graphed (see Fig. 2). The only parameter to be considered is R. For improved accuracy the influence of preheating upon the values of the thermophysical properties may also be taken into account.

In Ref. 5, analytic expressions linking the dimensionless power into workpiece to the dimensionless weld width on top surface, $\bar{Y}_M$, were presented for various weld cross-section shapes.

As an illustrating example, let us select a typical triangular cross-section profile, for which the following correlation is recommended in Ref. 5:

$$N = 2 + (0{\cdot}95 + 0{\cdot}835 Ph_\infty)\bar{Y}_M - (0{\cdot}168 + 0{\cdot}133 Ph_\infty)/\bar{Y}_M \tag{6}$$
$$\text{for } 0{\cdot}4 \le \bar{Y}_M \le 20$$

where

$$N = P_{KH}/\lambda_s(T_M - T_\infty)t \tag{7}$$

where $T_M - T_\infty$ is in K or °C (i.e. in degrees), P_{KH} = power into workpiece via keyhold (W) and t = weld depth (m).

With the notations:

$R = T_\infty/T_M$ (where T_∞, T_M are in °C; see the Appendix, eqn (A12)) and $Ph_\infty = Ph_o/(1 - R)$ (see the Appendix, eqns (A11), (A13) and (A14)).

Equations (6) and (7) lead to the following correlation:

$$\frac{P_{KH}}{t} = \lambda_s T_M (1-R)\left[2 + (0{\cdot}95 + 0{\cdot}835)\frac{Ph_o}{1-R}\right)\bar{Y}_M - \frac{0{\cdot}168 + 0{\cdot}133\dfrac{Ph_o}{1-R}}{\bar{Y}_M}\Bigg] \tag{8}$$

$$\text{for } 0{\cdot}4 \leq \bar{Y}_M \leq 20$$

$$T_M \text{ in } °C$$

The function P_{KH}/t versus $\bar{Y}_M$ is plotted in the nomograph of Fig. 2 (together with the $\bar{Y}_V(\bar{Y}_M)$ dependence). The values of the thermophysical properties in eqn (8) are considered known, so the only parameter involved is again R, the preheating parameter.

For constructing the nomograph of Fig. 2, the following data were used:

—material: 20 MnMoNi 55 alloy
—triangular weld cross-section profile
—$T_M = 1530\,°C$
—$T_V = 2800\,°C$
—$\lambda_s = 28\ W\ mK^{-1}$
—$\lambda_L = 23\ W\ mK^{-1}$
—$Ph_o = 0{\cdot}25$
—$L = 226{\cdot}5\ kJ\ kg^{-1}$
—$c_{p,s} = 600\ J\ kgK^{-1}$

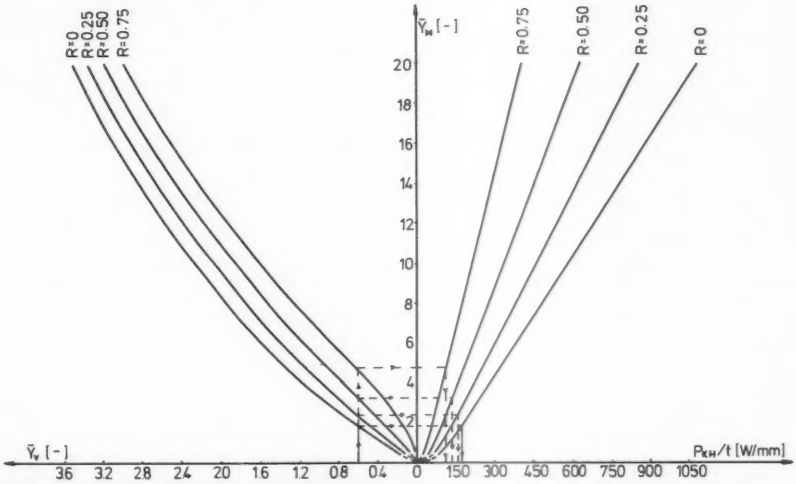

Fig. 2. Nomograph for determining the influence of workpiece preheating upon deep penetration welding results.

It is important to outline that the thermophysical properties of interest in our analysis do not change dramatically from one type of steel to another (calculations were made here for 22MnMoNi55 alloy). For this reason, the nomograph of Fig. 2 can be used for other steels as well.

The influence of workpiece preheating results from Fig. 2, which should be used as described below.

(1) Enter the nomograph at the appropriate $\bar{Y}_V$-value (for example, suppose that process parameters are within ranges so as to allow the approximation $\bar{r}_V = 1{\cdot}2\bar{r}_{1/e^2}$; $\bar{r}_{1/e^2}$ can be derived from the characteristics of the focusing system and the focus position with respect to the top surface of the workpiece.

$$\bar{Y}_V = 2{\cdot}4v(\bar{r}_{1/e^2})/a_s \tag{9}$$

(2) The straight line $\bar{Y}_V = \text{const.}$ intersects the $\bar{Y}_V(\bar{Y}_M)$ curves of different R-values.

(3) Find the corresponding $\bar{Y}_M$-values. As one can see, if only the preheating parameter R changes, an increase of preheating temperature leads to an increase of $\bar{Y}_M$. Weld widths are higher at higher R-values ($\bar{b}\nearrow$, as $\bar{Y}_M = v\bar{b}/a_s$, $v = \text{const.}$ and $a_s \simeq$ const.)

(4) For each $\bar{Y}_M$ obtained find the corresponding P_{KH}/t-value. One notices that an increase of R (all other parameters being kept constant) leads to a decrease of P_{KH}/t. At very low values of $\bar{Y}_V$, this absolute P_{KH}/t decrease is not accentuated, but the higher the $\bar{Y}_V$ values are, the more P_{KH}/t becomes sensitive to an R-increase.

As we assumed $ETE_{KH} = \text{const.}$ and as P_B and ETE_A also remain constant when the preheating temperature is varied, P_{KH} remains the same. The decrease of P_{KH}/t comes only from a t-increase.

EVALUATION OF EXPERIMENTAL RESULTS

The effects of stainless steel workpiece preheating upon weld geometry were investigated experimentally by Luciani *et al.*[7] An increase of weld width and depth was obtained when using an auxiliary power source together with a 450 W cw CO_2 laserbeam. The experimental results reported in the cited paper are in qualitative agreement with our theoretical predictions.

However, a quantitative evaluation of the measured values is not possible, because of the following reasons:

(1) Preheating was not uniform in the experiments. The theoretical model of our paper assumes uniform workpiece preheating.
(2) It is not clear whether steady state was reached or not in the experiments of Ref. 7; the model assumes steady state d.p.w.
(3) Steady state preheating temperature values are not reported.
(4) The ranges of parameters in Ref. 7 correspond to a region of the nomograph in Fig. 2 located in the nearest vicinity of the origin of the coordinate system (very low workpiece velocities, relatively low powers).
(5) Insufficient details are given about the power distribution in the focus (beam radii on the top surface of the workpiece). This information is needed for calculating the $\bar{Y}_V$-value to enter the nomograph in Fig. 2.
(6) Weld width values corresponding to each experimental run are not reported.
(7) The values of the keyhole power cannot be computed from the results reported in Ref. 7. Data about the weld cross section profile—whether a weld head was formed in the upper sheets of the workpiece or not at the lowest powers (low ETE_{KH} values would explain this behavior)—corresponding to each experimental run are not reported.

CONCLUSIONS

Preheating of the workpiece improves the deep penetration effect at welding of metals with high energy focused beams by two mechanisms. The first one is due to power transfer increase by keyhole efficiency improvement. The weld cross-section shape is expected to become more slender over the entire penetration depth by avoiding the formation of a weld head. The second mechanism is due to the modification of the heat conduction characteristics inside the workpiece (especially the effect of Ph_∞ increase). Its analytical evaluation is summarized in the nomograph of Fig. 2.

We do not share the opinion expressed in Ref. 7, where the deep penetration improvement by preheating is attributed to an increase of the absorption efficiency (see the interpretation of steady state absorption efficiency in this paper). Weld width increase by preheating can be useful in practice for example where adjacency imprecisions of the

pieces subject to welding have to be overcome. An increase of weld depth (by keyhole efficiency improvement or modification of the heat conduction characteristics) is a positive consequence of workpiece preheating.

Because of the fast decrease in the steady state temperature levels when moving off the beam impact region—which is specific to high energy focused beams processing—preheating can be restricted to a limited zone in the vicinity of the interaction region. The results of such a local preheating must be, in our opinion, similar to those obtained in the case of the entire workpiece being raised in temperature prior to processing (see also the experimental results reported in Ref. 7 and the effects of beam oscillation at electron beam welding described in Refs 8 and 9).

Further experimental work is needed to support the theoretical model of the present paper, parts of which were confirmed by experimental data given in Ref. 3.

REFERENCES

1. Swift-Hook, D. T. & Gick, A. E. F., Penetration welding with lasers. *Welding Research Supplement,* **11** (1973) 492–9.
2. Babenko, V. P. & Tychinskii, V. P., Gas jet laser cutting. *Sov. J. Quantum Electron,* **2** (1973) 399–410.
3. Peretz, R. & Mayer, H. G., Parameter correlations for deep penetration welding with high energy focused beams, *Optics and Lasers in Engineering,* **6** (1985) 225–50.
4. Peretz, R., Workpiece temperature distribution for deep penetration welding with high energy focused beams. *Optics and Lasers in Engineering,* **7** (1986/87) 69–81.
5. Peretz, R., New parameter correlations for deep penetration welding with high energy focused beams. *Optics and Lasers in Engineering,* (1988) (in press).
6. Hull, D. M. & Stewart, A., Laserbeam profiles-principles and definitions. *Lasers and Applications,* October (1985) 75–80.
7. Luciani, P. Y. Charissoux, C. & Calvet, J. N. CO_2 laser auxiliary source couplings: application to welding, *Proceedings of the 3rd International Conference on Lasers in Manufacturing, LIM-3 Paris, France* (1986) pp. 117–23.
8. Hehl, D., Die Beeinflussung der Aufschmelz- und Erstarrungsvorgänge beim Elektronenstrahlschweißen durch das Strahlpendeln, *IKE-Bericht* **3** (6), Stuttgart (1977).
9. Noller, F., Ein Elektronenstrahl hoher Richtwirkung als wesentliche Voraussetzung zum Elektronenstrahl-Tiefschweißen, *IKE-Bericht* **1** (9), Stuttgart (1979).

APPENDIX

From eqns (3) and (4) one obtains:

$$T_V - \bar{T}_P = (\bar{q}''/4\lambda_L)H_0(v\bar{r}_V/2a_s) \tag{A1}$$

The following relationship was derived in Ref. 4:

$$(T_M - \bar{T}_P)/(T_M - T_\infty) = \bar{q}''\lambda_s/\bar{q}'\lambda_L \tag{A2}$$

where $\bar{q}''$ is the power of the line source located at $x = 0$, $y = 0$ in the sheet $[o, dz]$ of the workpiece (phase change solid/liquid is taken into account). $\bar{q}$ is the component of $\bar{q}''$ which transfers to the solid part of the workpiece by heat conduction (sheet $[o, dz]$).

By eliminating the pole temperature $\bar{T}_P$ from the two equations above one gets.

$$\frac{T_V}{T_M - T_\infty} + \frac{\bar{q}''}{\bar{q}'} \cdot \frac{\lambda_s}{\lambda_L} - \frac{T_M}{T_M - T_\infty} = \frac{\bar{q}''}{4\lambda_L(T_M - T_\infty)} H_0(v\bar{r}_V/2a_s) \tag{A3}$$

Let us introduce the following dimensionless groups:

$$\theta_V = (T_V - T_M)/T_M - T_\infty) \tag{A4}$$

$$\bar{\eta}_V = v\bar{r}_V/2a_s = \bar{Y}_V/4 \tag{A5}$$

$$\bar{p}'' = \bar{q}''/\lambda_S(T_M - T_\infty) \tag{A6}$$

$$\bar{p}' = \bar{q}'/\lambda_S(T_M - T_\infty) \tag{A7}$$

into eqn (A3) for obtaining:

$$\theta_V = \frac{\lambda_s}{\lambda_L}\frac{\bar{p}''}{4}\left[H_0(\bar{Y}_V/4) - \frac{4}{\bar{p}'}\right] \tag{A8}$$

The expressions for p'_z and p''_z are given in Ref. 5 as functions of $Y_{z,M}$ the dimensionless weld width at location z. For $\bar{Y}_M$ (on top surface of the workpiece) within 'domain II' ($0{\cdot}4 \leq Y_M \leq 20$) the following analytic expressions should be used:

$$\bar{p}' = 2 + 1{\cdot}9\bar{Y}_M \tag{A9}$$

$$\bar{p}'' = 2 + (1{\cdot}9 + 1{\cdot}67Ph_\infty)\bar{Y}_M \tag{A10}$$

Similar correlations for other $\bar{Y}_M$ ranges of values (domains I, III) are given in Ref 5, though it should be outlined here that only the case detailed above (domain II) is frequently encountered in practice.

In eqn (A10), Ph_∞ is the phase change number of the material:

$$Ph_\infty = L/c_{p,s}(T_M - T_\infty) \tag{A11}$$

With the notations:

$$R = T_\infty / T_M \tag{A12}$$

where T_∞, T_M are in °C and

$$Ph_o = L/c_{p,s} \,.\, T_M \tag{A13}$$

where T_M is in °C, one may write:

$$Ph_\infty = Ph_o/(1 - R) \tag{A14}$$

Making use of the notation:

$$K = T_V / T_M \tag{A15}$$

where T_V, T_M are in °C and of eqns (A4), (A8), (A9), (A10) and (A14) one obtains the final result:

$$H_0(\bar{Y}_V/4) = \frac{1}{0{\cdot}5 + 0{\cdot}475\bar{Y}_M} + \frac{(\lambda_L/\lambda_s)(K-1)}{1 - R + 0{\cdot}4175 Ph_o \bar{Y}_M} \tag{A16}$$

$$\text{for } 0{\cdot}4 \leq Y_M \leq 20$$

The analytic expression of eqn (A16) correlates the beam radius on workpiece top surface to weld width at $z = 0$ and material properties (λ_L, λ_s, K, Ph_o). Effects of workpiece velocity are taken into account ($\bar{Y}_V$ and $\bar{Y}_M$ depend on this parameter) and the presence of R, the preheating parameter, allows for analysing the influence of workpiece preheating upon weld geometry.

Optics and Lasers in Engineering **9** (1988) 35–46

A Differential Interference Contrast System Incorporating a Murty Interferometer and Holographic Correction

K. Matsuda, M. Namiki & T. H. Barnes

Mechanical Engineering Laboratory, Namiki 1–2, Sakura-mura, Niihari-gun, Ibaraki-ken 305, Japan

(Received 19 August 1987; revised version received 27 October 1987; accepted 28 October 1987)

ABSTRACT

The Differential Interference Contrast (DIC) method, is useful for the observation of phase gradients in objects which have phase variations of less than one quarter of a wavelength. In this paper a description of an optical system in which the DIC method is realised through the use of a Murty-type shearing interferometer consisting of a plane parallel glass plate is given. This is then followed by a description of a modified version of this system, in which a holographic element is used to both compensate for lens aberrations, and also to modulate the output fringes in order to allow their easy detection. The application of this system to the measurement of film thickness is described, and results given which are in reasonably good agreement with measurements made on a Talysurf.

1 INTRODUCTION

The Differential Interference Contrast (DIC) method is similar to Zernike's phase contrast method,[1] and may be used for the observation of phase gradients in objects whose phase variations are less than one quarter of a wavelength. In this method, the wavefront from the phase object under test is divided by amplitude division, and a phase difference of $\pi/2$ introduced between the two resulting wavefronts. These wavefronts are then sheared relative to one another, and recombined to produce an interference pattern whose fringes carry information about the phase distribution of the object.

Optics and Lasers in Engineering 0143-8166/88/$03·50 © 1988 Elsevier Applied Science Publishers Ltd, England. Printed in Northern Ireland

In his book on interferometry, Steel[2] describes polarisation interference microscopes working on this principle, which have been developed by workers such as Françon and Normarski. This method has also been applied to the measurement of large phase objects, using holographic techniques.[3,4]

This paper describes a DIC system which incorporates a Murty-type[5] plane-parallel plate shearing interferometer, and shows how this system may be applied to film thickness measurement. It then gives a description of a modified version of the instrument in which holographic techniques are used for the compensation of lens aberrations,[6] and to provide a means of modulating the output interference fringes. This enables relatively poor quality optical components to be used in the instrument, and allows easy measurement of the relative phase of the output fringes, and hence the phase distribution across the object under test.

2 THE DIFFERENTIAL INTERFERENCE CONTRAST METHOD

For completeness a summary of the principle of the DIC method follows, before a description of how it is possible to realise this method using a Murty-type shearing interferometer.

To simplify the explanation, it is assumed an object with a rectangular phase distribution is used, as shown in Fig. 1a. The phase retardation introduced by the object is ϕ_f. The wavefront from the object is split into two by amplitude division, and a phase difference of $\pi/2$ introduced between the two resultant components. They are then sheared relative to one another by an amount Δs, and recombined to give the situation shown in Fig. 1b. On recombination, interference fringes are produced whose intensity distribution maps out the phase distribution of the object according to the familiar sinusoidal phase-intensity relationship shown in Fig. 1c. Thus, via this curve, the phase distribution of Fig. 1a gives rise to the intensity distribution shown in Fig. 1d.

Figure 2 shows how a Murty-type, plane-parallel shearing interferometer may be used to make a DIC system. Light from a He–Ne laser is expanded by a microscope objective and collimated by a good-quality lens, L. The collimated beam passes through the phase object, situated at S, and proceeds on to be reflected by both surfaces of the plane-parallel plate B (the Murty interferometer). Two output beams are produced, the relative shear between them being determined by the

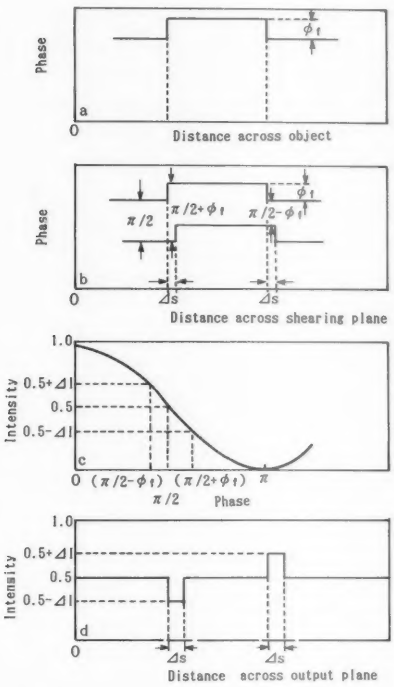

Fig. 1. The differential interference contrast method illustrated with a rectangular phase object.

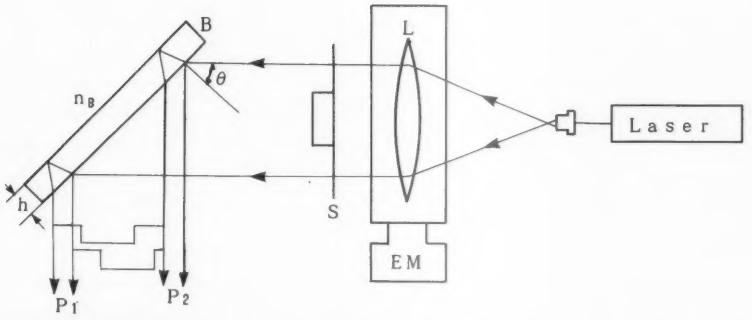

Fig. 2. Measurement of a phase object using a Murty-type shearing interferometer.

angle of the plate, it's thickness, and it's refractive index. A uniform phase delay is also introduced between the beams, which is critically dependent on the angle of the incident light onto the plate, θ. Thus, by altering this angle slightly, the phase difference between the output beams may be adjusted to be an odd multiple of $\pi/2$ without significantly affecting the shear. Of course, one way to adjust this phase difference would be to rotate the plate. However, the phase is so sensitive to angle that it was found easier to make this adjustment by laterally translating the collimator lens, L, perpendicular to the optic axis, using a micrometer stage EM.

It is easy to show that the path difference between the two output beams is given by:

$$D = 2h\sqrt{n_B^2 - \sin^2\theta} \tag{1}$$

Where: h = plate thickness,
n = plate refractive index,
θ = angle of the incident light (Fig. 2).

When θ changes by a small amount $\Delta\theta$, the change in D may be obtained by differentiating:

$$\Delta D = \frac{-2h \sin^2\theta \Delta\theta}{\sqrt{n_B^2 - \sin^2\theta}} \tag{2}$$

Now if the lens is translated by a small amount x, and it's focal length is f, then $\Delta\theta \doteq x/f$, and:

$$\Delta D \doteq \frac{-2h \sin^2\theta}{\sqrt{n_B^2 - \sin^2\theta}} \frac{x}{f} \tag{3}$$

If x is small compared to f, and θ is large, so that it's fractional change is small for this amount of lens translation, then ΔD, and therefore the phase difference between the output beams from interferometer, is approximately proportional to x. This can be used to operate the system in a dynamic, rather than a static, fashion. As the lens is translated and the path difference changes (the shear also varies, but for small translations this effect may be neglected) the fringes move across the output field. There is a phase difference between the signal at p_1 and that at p_2, which is proportional to the film thickness. Let $\phi_p(x)$ be the phase difference introduced between the output beams, by the Murty plate (in the conventional DIC method this would be fixed at $\pi/2$). Now if ϕ_f is the phase retardation introduced by the film, then the fringe phase at p_1 will be:

$$\phi_{p_1} = \phi_p(x) + \phi_f \tag{4}$$

and that at p_2 will be:

$$\phi_{p_2} = \phi(x) - \phi_f \tag{5}$$

The phase difference between the two fringe signals is therefore:

$$\Delta\phi = 2\phi_f \tag{6}$$

and the film thickness may be obtained from:

$$d = \frac{\Delta\phi\lambda}{4\pi(n-1)} \tag{7}$$

Where: d = film thickness,
n = film refractive index,
λ = wavelength used (632·8 nm),
$\Delta\phi$ = fringe signal phase difference.

Any one of several different methods could be used to measure the phase difference between the two fringe signals. The signals were logged as the lens was translated, and the phase difference determined from measurements made on the two intensity profiles so obtained.

3 INITIAL EXPERIMENTS

To test the above ideas, and to show how this method may be used to measure film thickness, initial experiments were conducted using the set-up shown in Fig. 3. The light source was a 50 mW He–Ne laser ($\lambda = 632{\cdot}8$ nm), and the collimator lens, L ($f = 1000$ mm) was mounted on a motor driven micrometer stage EM (Microdex-2, Aerotech Inc., Pittsburgh, USA). The stage could be moved in steps of 2 μm. In the output plane, light passed through pinholes p_1 and p_2 (1 mm in diameter) to be collected by lenses and detected by photodetectors PD_1 and PD_2. The phase difference between the detector signals was determined by moving the lens, logging the detector outputs, and analysing them using the signal analyser.

The amount of shear was adjusted by rotating the Murty plate. In order to avoid the detrimental effects of air movement, it is desirable that the shear be as small as possible, provided there is sufficient light for satisfactory fringe measurements. In our set-up, the shear was set at 2 mm, and at each measurement point 1000 samples were taken over several tens of seconds to average out the effects of turbulence.

The arrangement of the film samples is shown in Fig. 4. The samples used were MgF_2 films deposited on plane-parallel glass substrates. The film occupied the centre of the substrate only, with sufficient room

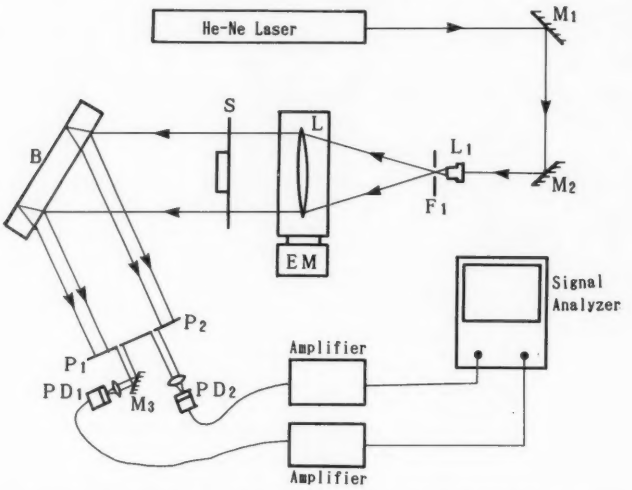

Fig. 3. The optical set-up for the initial experiments (no holographic compensation).

being left at the edges to generate the step-like phase profile required for operation of the instrument.

Table 1 shows the results obtained with this set-up. In all, five samples were measured, and the measurements obtained with the DIC instrument compared with those obtained using a Talysurf, type 5–120. Table 2 shows the way in which the results obtained for one film varied depending on the number of samples taken at each measurement point. From these results it was concluded that air movements gave rise to an error of the order of 5 nm or so.

The results obtained with the DIC instrument differ somewhat from those obtained with the Talysurf. Apart from the possibility that the assumption for the refractive index of the film might be slightly in error,

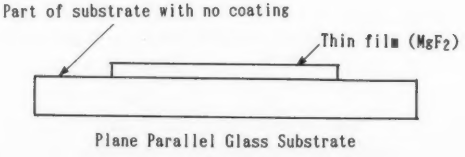

Fig. 4. The thin film sample.

TABLE 1
Experimental Results Obtained with the Set-up of Fig. 5

	Talysurf (nm)	*DIC (nm)*
Sample A	about 130	142
Sample B	about 80	112
Sample C	about 40	54
Sample D	about 20	42
Sample E	about 10	25

TABLE 2
The Effect of Varying the Number of Samples Averaged for each Reading

Sampling points N	*Measured film thickness (nm)*
100	143
200	137
500	142
1000	142

this may be due to a variety of effects including:

(1) The deformation and damage caused to the surface by the Talysurf needle.
(2) Air movements.
(3) Non-uniformities in the film substrates and the Murty plate.

Other considerations included the effects of multiple reflections in the film, and spurious phase changes caused by absorption. However, it was concluded that these effects were negligible.

4 THE USE OF HOLOGRAPHIC TECHNIQUES

In order for the method described above to work satisfactorily, the collimating lens, L (Fig. 3) must be of good quality. Since the instrument incorporates a shearing interferometer, any wavefront aberrations will affect the output fringe pattern, and hence the results. However, the use of a good quality, long focal length collimator makes the instrument large and heavy. It was therefore decided to use a small,

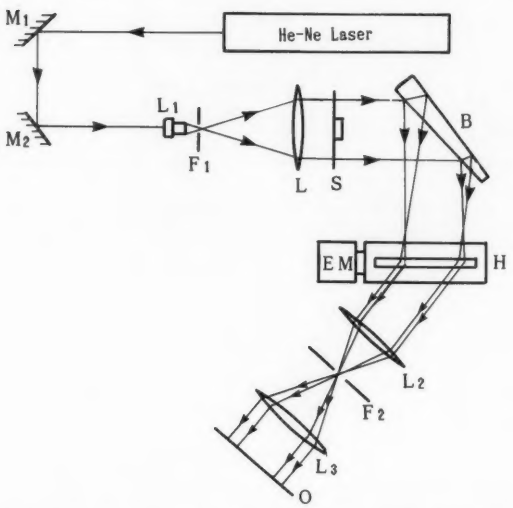

Fig. 5. The DIC interferometer with holographic correlation and fringe scanning.

large aperture, lower quality lens, and to correct its aberrations holographically.[6] At the same time, it was found possible to move the hologram rather than the collimating lens, to modulate the fringes in the output plane to allow their phase measurement.

The principle of operation of the holographically compensated instrument is shown in Fig. 5. As before, the beam from the laser is expanded and nominally collimated by the now rather poor collimating lens L. It then passes through the sample S in the normal way, and proceeds to the shearing plate B. However, the shearing plate is now wedged, and the two reflected beams carry on towards the hologram H, travelling at different angles. The hologram is made using these two beams as object beams, and a perfect plane wave as the reference beam. Thus, when illuminated with the two beams from the shearing plate alone, each of these beams reconstructs the reference wave. The two reconstructions are, of course, superimposed except for the shear, and travel on to be collected by lens L_2 eventually to interfere in the output plane O. Unwanted diffracted orders are filtered out by pinhole F_2.

Now the hologram is a grating, and one of the output beams from the instrument corresponds to +1 order diffraction, whilst the other corresponds to −1 order diffraction. Thus, when the hologram is moved

laterally, a phase shift is introduced between these two beams that cause the output fringes to be modulated. The film thickness may now be determined by electrical phase measurement, in a method analagous to that described in section 2 above, except that now the hologram is moved rather than the collimating lens. Provided the movement of the hologram is limited, and the aberrations of the collimating lens are not too large, any deviations from perfect aberration correction, caused by movement of the hologram away from it's 'correct' position, will be negligible.

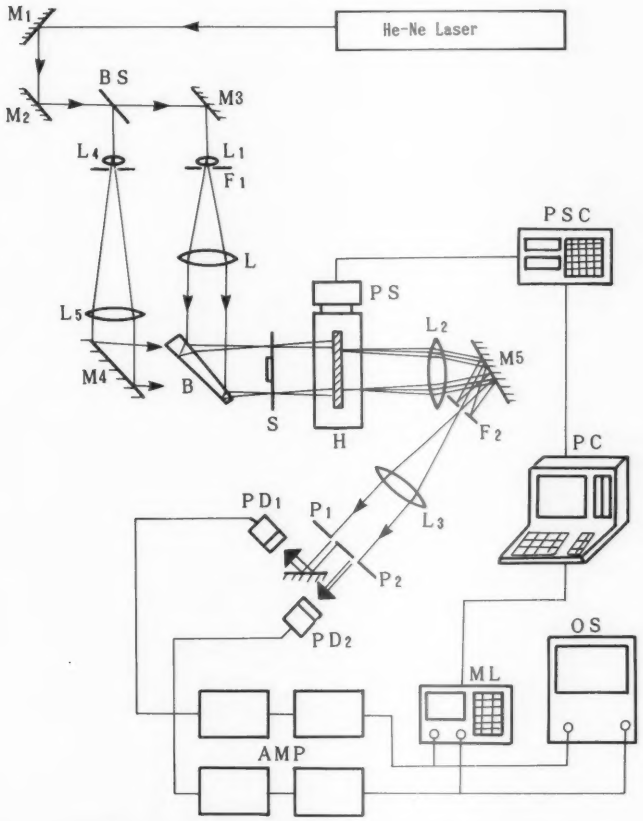

Fig. 6. The holographically compensated set-up used for the final experiment.

5 EXPERIMENTS WITH THE MODIFIED SYSTEM

The experimental set-up used to demonstrate the holographic system is shown in Fig. 6. This is essentially the same as Fig. 5, but with the addition of the optics for generating the hologram reference beam, and the measuring electronics.

The reference beam is derived from a beamsplitter BS, and expanded by L_4 and L_5 before being reflected by M_4, to pass through the shearing plate B, to make the hologram H. The two object beams are derived by reflection from the wedged shearing plate as described above. The hologram was made without the sample S in the system. For high diffraction efficiency, the Kodak reversal bleach process was used.

The shear in this system was set at 3·8 mm, and the output fringes were detected by the two photodetectors PD_1 and PD_2 behind 1 mm diameter pinholes. The photodetector signals were amplified and sampled by a data logger ML, and at the same time observed on an oscilloscope. The hologram was mounted on a pulse stage PS (Aerotech ATS-302 MMS) controlled by a stepper controller PSC (Aerotech Unidex II). The stepper controller itself was controlled by a personal computer.

Figure 7 is a photograph of the output field of the system, and the circular intensity patterns quite clearly demonstrate the DIC phenomenon. Table 3 shows the results of film thickness measurements made with the system. The same set of samples as before were used in this experiment.

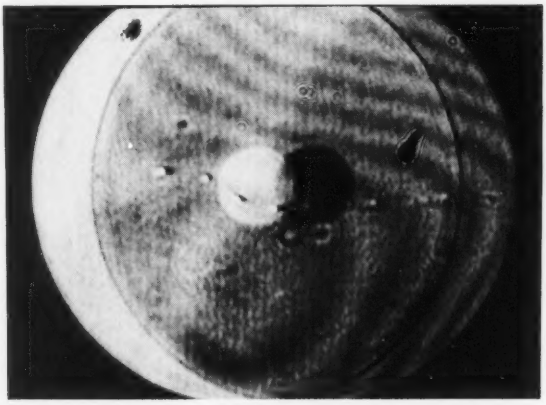

Fig. 7. A photograph of the output plane of the DIC system.

TABLE 3
Experimental Results Obtained with the Holographically Compensated Set-up of Fig. 6.

	Talysurf (*nm*)	*DIC* (*nm*)
Sample A	about 130	132·7
Sample B	about 80	83·0
Sample C	about 40	55·8
Sample D	about 20	34·6
Sample E	about 10	16·4

6 CONCLUSION

We have described a Differential Interference Contrast method of measuring phase objects which uses a Murty-type shearing interferometer. We have also described a modification of this system which uses a moving hologram for aberration compensation and fringe modulation. This technique allows the use of lightweight, small, inexpensive optical components whilst maintaining the accuracy of the instrument. The application of the method to film thickness measurements has also been described.

ACKNOWLEDGEMENTS

The authors gratefully acknowledge the helpful discussion of Mr K. Hibino and the assistance of Mrs H. Kubota and Mrs M. Tasuno of the Mechanical Engineering Laboratory.

REFERENCES

1. Born, M. & Wolf, E., *Principles of Optics*. Pergamon Press. New York, 1956, pp. 423–7.
2. Steel, W. H., *Interferometry*. Cambridge University Press. 1967, pp. 178–82.
3. Gorlitz, D. & Lanzl, F. Introduction of phase bias in coherent differentiation filtering. *J. Optics* (*Paris*), **8** (1977) 289–95.
4. Matsuda, K. & Namiki, M., Holographic lateral shear interferometer for differential interference contrast method. *J. Optics* (*Paris*). **11** (1980) 81–5.

5. Murty, M. V. R. K. & Malacara, D., Some applications of the gas laser as a source of light for the testing of optical systems. *Japanese J. of Appl. Phys.*, **4,** supplement 1 (1965) 106.
6. Matsuda, K., Watanabe, S., & Eiju, T., Real time measurement of large liquid surface deformation using a holographic shearing interferometer. *Appl. Opt.* **24** (1985) 4443–7.

Optics and Lasers in Engineering **9** (1988) 47–55

Frozen Strain Moiré Used in the Analysis of Impact Loading

J. W. Tong,* H. Q. Li & Y. Q. Jia

Department of Mechanics, Tianjin University, Peoples Republic of China

(Received 2 September 1987; revised version received and accepted 9 November 1987)

ABSTRACT

This paper presents a solution to the problem of the displacement fields and strains in a semi-infinite plate with two half-circular holes during the propagation of a stress wave. The solution was realized experimentally by means of the method of the frozen strain moiré using a double-pulse ruby laser. The load of impact was applied by a pendulum hammer. Two suitable external-trigger mechanisms were used to fire the ruby laser at predetermined intervals. The moiré fringe patterns of the U and V displacement fields were recorded on a holographic film adhered to the specimen at different time delays after impact.

INTRODUCTION

The solutions to the problem of principal stress distribution in dynamic loading during the propagation of a stress wave were presented previously. The solutions were found by means of holographic photoelasticity utilizing a Faraday Rotator in an optical arrangement,[1] by holo-interferometry using the reflected light and photoelasticity using the transmitted light.[2]

A replica technique is used for applying a 40 lines/mm black-and-white crossed grating to specimens using photoresist, silicone rubber and epoxy resin by C. A. Walker and J. McKelvie.[3]

A cross-line grating was made using a design of optical arrangement

* Present address: CCR ED 45, 2/020 Ispra (Varese) Italy.

Optics and Lasers in Engineering 0143-8166/88/$03·50 © 1988 Elsevier Applied Science Publishers Ltd, England. Printed in Northern Ireland

and the technique[4] of sticking holographic film to the specimen so that moiré fringe patterns could be obtained for the U and V displacement fields. The method of the frozen strain moiré to be described here is employed to measure U and V of the in-plane displacement, where U and V are displacement components in the X- and Y-directions respectively.

EXPERIMENTAL APPARATUS

Shock generator

As shown in Fig. 1, the stress pulse was applied on a small region of one edge of a semi-infinite plate by the impact of a concentrated force utilizing a reproducible pendulum hammer. The mechanism provides an accurately reproducible stress pulse.

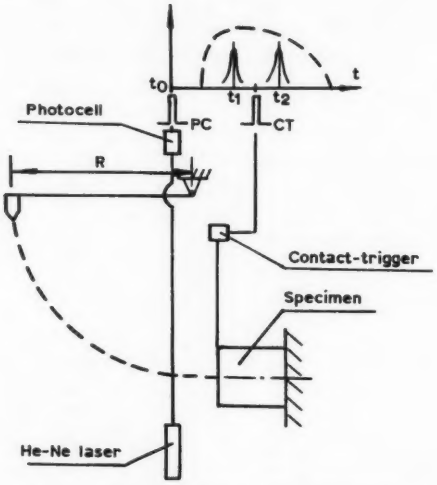

Fig. 1. Triggering and synchronizing system.

Triggering and synchronizing system

As shown in Fig. 1, the beam of a He–Ne laser is cut off when the hammer passes point zero, and as a result one electro-pulse PC is emitted by the photocell to trigger the ruby laser. This is called the time t_0 of pulse PC. The first exposure time t_1 of the ruby laser is ordered by

the pulse PC. When the hammer contacts the specimen, another electro-pulse CT is also emitted to the ruby laser by the contact-trigger. The second exposure time t_2 of the ruby laser is ordered by the pulse CT. The times t_1 and t_2 are independent. An interval between the hammer contacting the specimen and the second exposure time t_2 is accurately delayed. On the other hand, we can change the second exposure time t_2 using the control of the ruby laser, so that the time delay can be varied.

The optical arrangement for recording the moiré fringe patterns

As shown in Fig. 2, two symmetrical beam paths are employed to make a cross-line grating. If the mirrors M_1 and M_2 are moved out of the beam paths, the grating of the Y-direction is generated. The grating of the X-direction is formed when the mirrors M_1 and M_2 are moved into the beam paths. If change beam splitters for the mirrors M_1 and M_2 as well as the mirrors M_3 and M_4 are moved out of the beam paths, the gratings of the X- and Y-directions can be obtained simultaneously. A photograph of the experimental set-up is shown in Fig. 3.

The laser used was a ruby laser with output 0·5 J per pulse. The wavelength λ of the light of the ruby laser was 694·3 nm. A organic glass specimen is shown in Fig. 4. The holographic film of type 3 which is made in China is cemented on the surface of the specimen by adhesive of type TD-2 made in Tianjin University. The double-exposures are made respectively to non-loaded and loaded specimens on the same holographic film. After peeling the holographic film from the specimen,

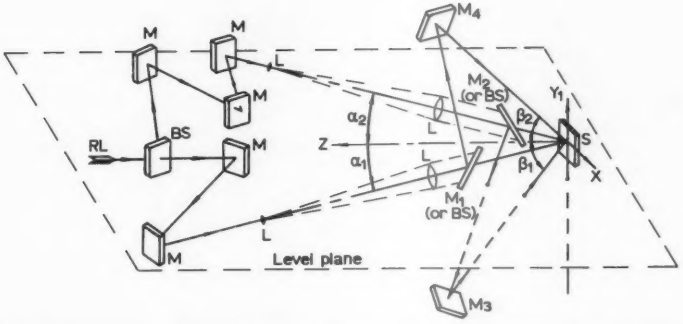

Fig. 2. The optical arrangement: RL-ruby laser; BS-beam splitters; M, M_1, M_2, M_3 and M_4-mirrors; S-specimen; L-lenses.

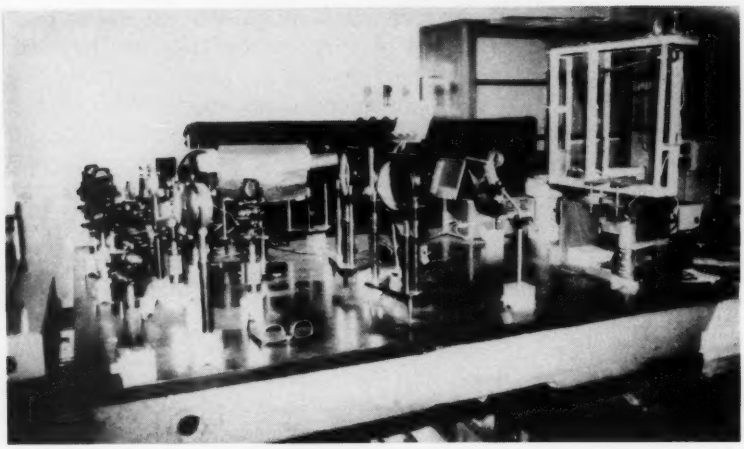

Fig. 3. Experimental set-up.

the holographic film is developed and fixed. We clip the holographic film between two transparent glass plates after drying the holographic film. We can observe the U and V displacement fields when the observations are located respectively in the XZ- and YZ-plane, with white light illumination transmitted through the holographic film. The

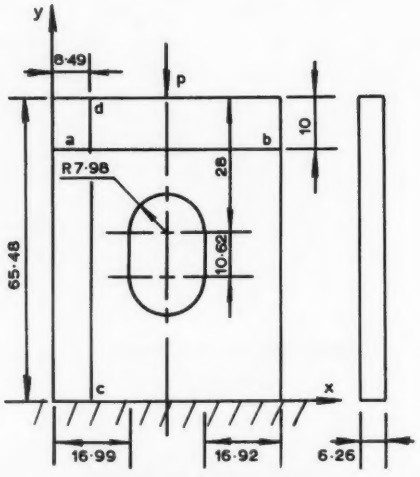

Fig. 4. Size of the specimen.

U and V displacement fields' appearances are given by[5]

$$\left.\begin{aligned} U &= \frac{n_x}{f_x} - d\alpha(\cos\alpha_1 - \cos\alpha_2)\frac{x'}{f_x\lambda} - \Delta z(\cos\alpha_1 - \cos\alpha_2)\frac{1}{f_x\lambda} \\ V &= \frac{n_y}{f_y} - d\beta(\cos\beta_1 - \cos\beta_2)\frac{y'}{f_y\lambda} - \Delta z(\cos\beta_1 - \cos\beta_2)\frac{1}{f_y\lambda} \end{aligned}\right\} \quad (1)$$

We employ two symmetrical beam paths ($\alpha_1 = \alpha_2$ and $\beta_1 = \beta_2$) in the XZ- and YZ-plane. Equation (1) may be written

$$\left.\begin{aligned} U &= \frac{n_x}{f_x} \\ V &= \frac{n_y}{f_y} \end{aligned}\right\} \quad (2)$$

The frequencies of virtual cross-line grating are given by $f_x = 675$ lines/mm and $f_y = 672$ lines/mm.

EXPERIMENTAL RESULTS

The frozen moiré fringe patterns are recorded at 23, 33, 43 and 53 μs after impact. They are shown in Fig. 5 where Fig. 5(a) and Fig. 5(b) express respectively the displacements U and V.

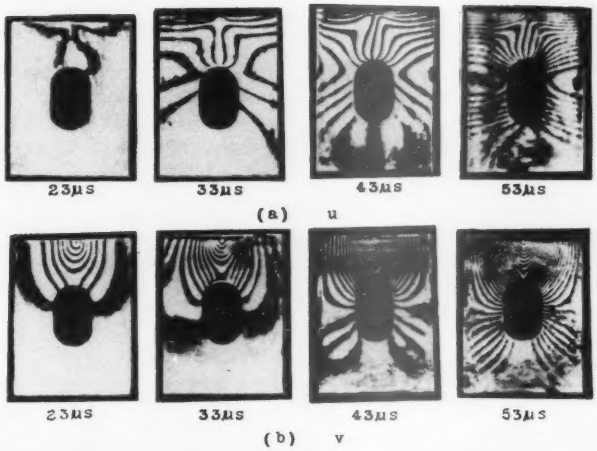

Fig. 5. The frozen moiré fringe patterns after impact.

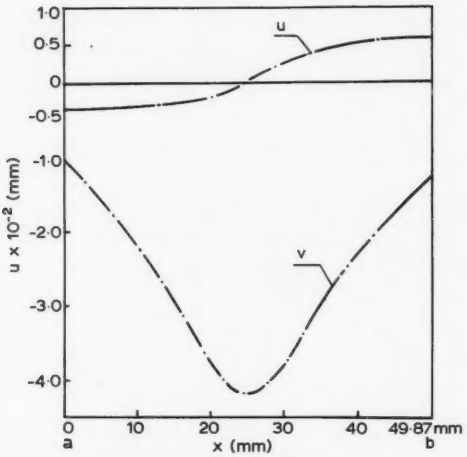

Fig. 6. The U and V displacement fields on the section a–b.

The U and V displacement fields on the sections a–b and c–d recorded at time delay 53 μs after impact are shown in Figs 6 and 7.

The U and V displacement fields on the boundary of the hole at time delay 53 μs after impact are shown in Figs 8 and 9.

A polynomial was used to express the U and V displacement functions from the experimental data, using microcomputer programs. We obtained normal strains and two cross-derivatives ε_x, $\partial v/\partial x$ on the section a–b and ε_y, $\partial u/\partial y$ on the section c–d for a time delay of 53 μs

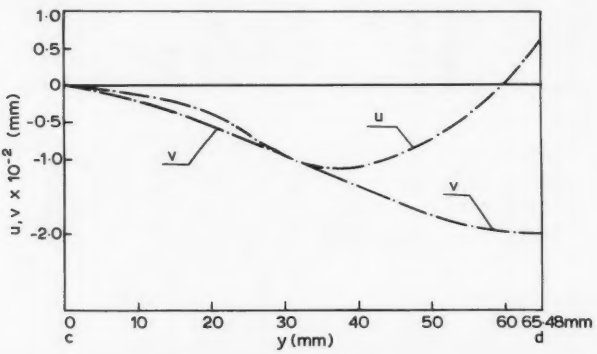

Fig. 7. The U and V displacement fields on the section c–d.

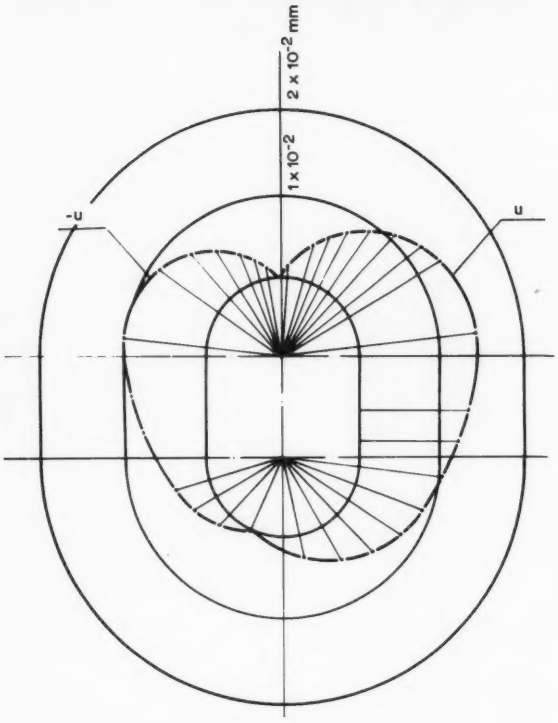

Fig. 8. The distribution of the displacement U on the boundary of a hole.

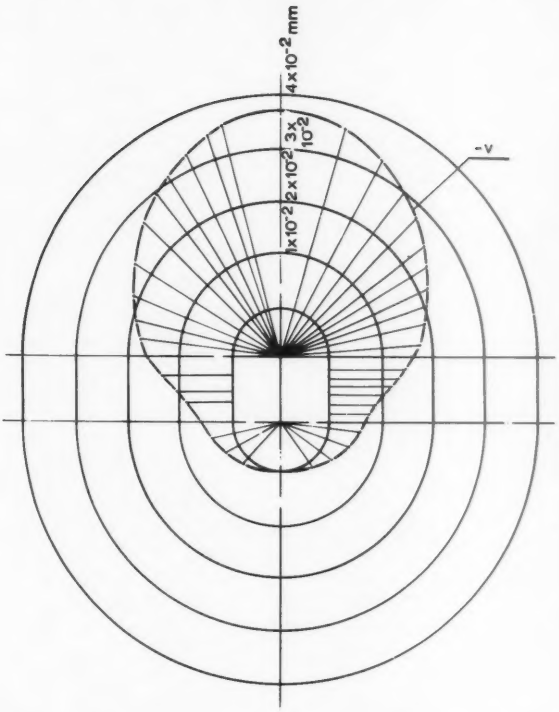

Fig. 9. The distribution of the displacement V on the boundary of a hole.

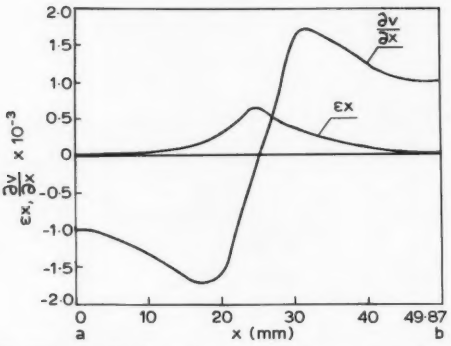

Fig. 10. The distribution of ε_x and $\partial v/\partial x$ on the section a–b.

after impact. They are shown in Figs 10 and 11. The section a–b intersects the section c–d and the strains of intersection are given by

$$\varepsilon_x = \quad 0.0495 \times 10^{-3},$$
$$\varepsilon_y = -0.1970 \times 10^{-3},$$
$$\gamma_{xy} = \quad 0.4970 \times 10^{-3}.$$

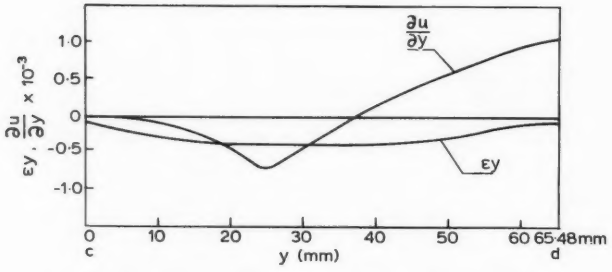

Fig. 11. The distribution of ε_y and $\partial u/\partial y$ on the section c–d.

CONCLUSION

The benefits of the frozen strain moiré method are that it can be used with an opaque specimen, the times of experimental progress are shorter and the contrast of the moiré fringe patterns are better. On the other hand, this method has limitations because the adhesive must be strong enough to transmit the deformation of the specimen to the

holographic film but be weaker than the holographic film to allow it to be peeled easily.

The results of this investigation indicate that the interval between the firing of the ruby laser and the hammer contacting with the specimen is stable. This shows that, before the hammer contacts the specimen, the velocity of the hammer is stable. So the precisely reproducible loading of impact was obtained by means of a well designed pendulum hammer. The triggering of the double-pulse ruby laser can be accurately timed by the photo-trigger and contact-trigger.

REFERENCES

1. Chia, Y. C., Tong, J. W. & Tou, C. T., A study of dynamic holographic photoelasticity using ruby laser. *Transactions of the CSME,* **8** (1984) 117–20.
2. Tong, J. W. & Li, H. Q., Dynamic stress analysis using simultaneously holo-interferometry and photoelasticity. *Opt. and Lasers in Engng,* **6** (1985) 145–56.
3. Walker, C. A. & McKelvie, J., A practical multiplied-moiré system. *Experimental Mechanics,* **18** (1978) 316–20.
4. Luo Zhishen, Yuan Fuxiang, Liu Wenxiu & Zhang Guiqin, Some improvements of moiré interferometry. In *Proceedings of the International Conference on Experimental Mechanics,* Beijing, Science Press, Beijing, China, 1985, pp. 446–53.
5. Tong, J. W. & Li, H. Q., Dynamic moiré interferometry. In *Proceedings of the 5th Conference of China on Experimental Mechanics,* Nanjing Institute of Aeronautics, Nanjing, China, 1987.

Optics and Lasers in Engineering **9** (1988) 57–59

Research Note

Designed Experiments with a Laser Dilatometer

We recently described a laser dilatometer in which light interference is used to measure temperature induced dimensional changes in objects.[1] The specimen to be measured is in vacuum. The temperature range is from 20 to 800 °C. Heating is accomplished in a two-zone furnace with a temperature control unit ensuring accuracy in maintaining a constant temperature of ±0·1 °C. A 5 mW He–Ne laser is used. The resolution of elongation measurement is $\lambda/50$.

The dimensional changes in isotropic solids under the impact of temperature are characterized by the mean linear thermal expansion coefficient (LTEC) $d = (1/L_T)(\delta L/\delta T)$, where L_T is the object length at temperature T, and δL and δT are the changes in length and temperature, respectively.

When reversible thermal changes in a given material are studied, an analytical expression is sought which approximates LTEC as a function of temperature in the range of interest. In determining LTEC, both the control variable (temperature) and the response (elongation) are measured with random error. It is assumed that systematic errors are eliminated or taken into account. It is well known how the least squares method works; it is based on multiple measurements. In dilatometry the experimental data are best described by a polynomial of third degree:

$$y = \delta L = a_0 + a_1(T - T_0) + a_2(T - T_0)^2 + a_3(T - T_0)^3 \qquad (1)$$

The least squares method gives the best unshifted and consistent estimates of the coefficients a_i. However, another statistical approach is also feasible: experimental design or planning of experiments. What is gained is the best solution with minimum experimental efforts. This new approach drastically changes the experimental strategy. It is proved that the best estimates of the regression coefficients, obtained by a designed experiment, minimize the residual variance, i.e. they coincide with the estimates from the least squares method.[2]

Quite appropriate for dilatometric measurements are the D-optimal

Optics and Lasers in Engineering (**9**) (1988)—© 1988 Elsevier Applied Science Publishers Ltd, England. Printed in Northern Ireland

experimental designs. This is a set of values in a preliminary selected interval for the independent variable (in our case, temperature), specifying the points of carrying out the experiment. *D*-optimal plans produce such estimates for '*a*' in eqn. (1), that the covariance matrix has a minimal determinant, i.e. they minimize the residual variance. The number of measurements is equal to the number of regression coefficients which must be determined.

The plans (T^i_{plan}), variance matrices ($\hat{D}$), and matrices ($\hat{M}$) translating the measurements into regression coefficients estimates, are evaluated on a computer and are presented in tables.[3] In all plans the variable is normalized in the interval $\{-1, +1\}$. To perform the experiment, a plan translation must be accomplished in the range of interest $\{A, B\}$:

$$T^i_{\text{plan}}\{-1, +1\} \leftrightarrow T^i_{\text{exp}}\{A, B\}$$

with

$$T^i_{\text{exp}} = (A + B)/2 * (B - A)/2 * T^i_{\text{plan}}$$

where T^i_{exp} are the actual experimental temperatures ($i = 1$ to 4), and T^i_{plan} is the ith value of the normalized variable indicated in the plan.

For a regression surface of the form of eqn. (1) four measurements are required. The elongation must be evaluated at normalized temperatures:

$$T^i_{\text{plan}} = (-1; -0{\cdot}447; +0{\cdot}447; +1)$$

After the experiments, the vector of results $\bar{\mathbf{C}}$ is constructed. In our case the vector has four components, one for each measurement. Multiplying matrix $\hat{M}$ by the vector of results $\bar{\mathbf{C}}$ yields an estimate for the vector of the regression coefficients $\bar{\mathbf{a}} = \hat{M} * \bar{C}$, or

$$\begin{bmatrix} a'_0 \\ a'_1 \\ a'_2 \\ a'_3 \end{bmatrix} = \begin{bmatrix} -0{\cdot}1248 & 0{\cdot}6248 & 0{\cdot}6248 & -0{\cdot}1248 \\ 1{\cdot}1248 & -1{\cdot}3978 & 1{\cdot}3978 & -0{\cdot}1248 \\ 0{\cdot}6248 & -0{\cdot}6248 & -0{\cdot}6248 & 0{\cdot}6248 \\ -0{\cdot}6248 & 1{\cdot}3978 & -1{\cdot}3978 & 0{\cdot}6248 \end{bmatrix} \cdot \begin{bmatrix} c_0 \\ c_1 \\ c_2 \\ c_3 \end{bmatrix}$$

Then a reverse translation of the temperature variable is accomplished, so that it varies in the range $\{A, B\}$. Along with the experimental design, the covariance matrix $\hat{D}$ is also given:

$$\hat{D} = \begin{vmatrix} 3{\cdot}248 & 0 & -3{\cdot}748 & 0 \\ 0 & 15{\cdot}757 & 0 & -16{\cdot}257 \\ -3{\cdot}741 & 0 & 6{\cdot}247 & 0 \\ 0 & -16{\cdot}257 & 0 & 18{\cdot}756 \end{vmatrix}$$

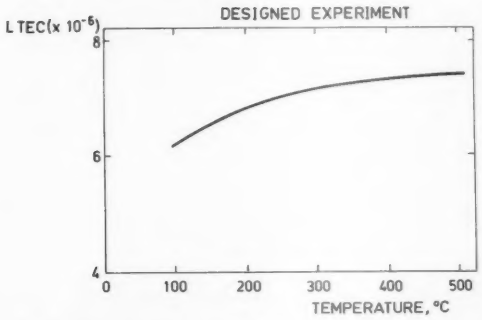

Fig. 1. Elongation versus temperature of a quartz sample in the range 100–500 °C and estimates of the coefficients of the third-degree polynomial $a'_0 = 7{\cdot}2093$, $a'_1 = 0{\cdot}3939$, $a'_2 = -0{\cdot}3593$, $a'_3 = 0{\cdot}2961$.

The diagonal elements of this matrix give an estimate of the error in the regression coefficients as determined. The non-diagonal elements are a measure of the correlation between two coefficients.

Using the experimental plan and the matrix $\hat{M}$ the regression coefficients of eqn. (1) for a quartz sample are determined. The measurements were performed on a laser dilatometer in the temperature range 100–500 °C. The quartz specimen in the form of a hollow prism was placed between two polished quartz plates in vacuum. The dimensional change was measured interferometrically. Results are presented in Fig. 1.

So the mathematical theory of experiments brought about essential changes in the experiment itself. *D*-optimal plans are extremely useful in laser dilatometry in order to get accurate estimates (in the sense of least squares) with minimum experiments.

REFERENCES

1. P. Sharlandjiev, G. Mintchev, M. Gospodinov and A. Slavtcheva, *Opt. Lasers Eng.*, **7** (1986/7) 91.
2. R. Farvel, J. Kiefer and A. Walbran, *Proc. 5th Berkeley Symp. Statistics and Probability*, Vol. 1, 1967, p. 113.
3. I. Dubova, T. Ptzalidze and V. Feodorov, *Tables of D-opt. plans*, preprint N: 16, ed. Moscow University, 1970.

P. Sharlandjiev & A. Slavtcheva
Central Laboratory for Optical Storage and Processing of Information, PO Box 95, Sofia 1113, Bulgaria

(Received 25 July 1986; revised version received 13 July 1987; accepted 14 July 1987)

Optics and Lasers in Engineering **9** (1988) 61–63

Conference Report

THIRD ALVEY VISION CONFERENCE, 15–17 SEPTEMBER 1987, UNIVERSITY OF CAMBRIDGE

The Alvey Programme is funded by the UK Government to promote research in Information Technology. Some 200 co-operative projects between industry and academia cover research in five main areas: Very Large Scale Integrated circuits (VLSI), Software Engineering, Systems Architecture, and the areas where vision projects are funded, Intelligent Knowledge Based Systems (IKBS), and the Man/Machine interface (MMI).

The Alvey Vision Club was set up to act as a forum for the exchange of research experience and results amongst its members, discussion of future research directions, dissemination of information on research external to Alvey (arising from overseas visits and conferences) and acts as a contact point for other research workers. Membership of the Club is open to all active workers on vision-related Alvey funded projects; however, the conferences are open to anyone with an interest in image processing and computer vision. The annual three-day Conference contains co-ordinated presentations from the major projects, in addition to invited papers and other papers from the field of image processing, including human cognition.

This year a wide range of topics was discussed, covering both software and hardware, with applications from both computer science and human physiology including object recognition in 2 and 3D for both stereo images and time sequences, fast hardware for vision, systems for industrial inspection, stereo matching using transputers, networks for vision problems, the human primal sketch, the use of colour, knowledge based segmentation for remote sensing, relaxation labelling, a review of Hough Transform methods and 'snakes'—contour models which are fitted to edges in images by grey-scale gradient climbing techniques, and subsequently 'cling' to it through a sequence of images.

The Program Chairman was J. P. Frisby, University of Sheffield, who

Optics and Lasers in Engineering (**9**) (1988)—© 1988 Elsevier Applied Science Publishers Ltd, England. Printed in Northern Ireland

introduced the first session beginning with the consortium who are trying to identify objects in 2D images. This was illustrated by attempting to recognise a vehicle in a general daylight scene, using prior knowledge about commonly occurring objects in the scene and the contexts in which they are most likely to be found, e.g. if this blue patch is sky, then this white patch is more likely to be a cloud than a car.

Speakers from IBM UK Scientific Centre Winchester and the A1 Vision Research Unit at Sheffield explained their research into the recognition of manufactured objects in 3D images, including the identification of edges using stereo cameras, leading to a description of the scene geometry, identification with expected objects already stored as models in the computer, and better methods of representing those models. This was demonstrated by guiding a robot arm in a pick and place task.

An evening session began with a speaker from the Department of Trade and Industry, describing their mechanisms for exploitation of Vision Research, which prompted some lively discussion. B. Ford, NAg Ltd described the IPAL (Image Processing Algorithms Library) project, which is trying to collect algorithms and mould them into a portable, robust, well documented subroutine library which will be readily available to image processing research after the end of the Alvey funding. M. B. Brown (British Aerospace, Chairman of the Club), then led a debate on 'Whither the Alvey Vision Club?', asking the members whether we should attempt to prolong our existence beyond the end of the main Alvey funding, or whether some other national association might be asked to take over our role.

The first invited speaker, O. Faugeras, INRIA, described work on an ESPRIT project in 3D vision, building a mobile robot, with three cameras, capable of understanding indoor scenes sufficiently well that it can both recognise objects and avoid them. 'Structure from motion' and 'optic flow' are the main techniques used, with an additional probability component to cope with the uncertainties of the sensing, even with three cameras. Future work will concentrate on improving the low level algorithms to identify edges, regions, colour, textures etc. and to use a greater degree of abstraction, i.e. to recognise an object as a chair, even when it's geometric description is not identical with that of the stored chair.

The second invited speaker, H.-H. Nagel (Karlsruhe), described the extraction of conceptual descriptions of a scene from image sequences. An episode extraction system, EPEX, links related motions, e.g. those needed to park a car, and stores them in a database. The German

natural language system, CITYTOUR, is being developed at Saarbrucken to use the database to answer queries about several related moving objects, simple dialogue is possible now, of the form:

Did the tram stop at the tramp stop?—No, it went past it.

The aim is to build an unattended monitoring system for busy city intersections.

K. M. Crennell

Future conference

The next Conference, AVC88, is planned for September in Manchester. The Program Chairman is C. J. Taylor, Department of Medical Biophysics, University of Manchester. For further information contact the Alvey Vision Club Secretary: K. M. Crennell, Informatics Department, Rutherford Appleton Laboratory, Chilton, Didcot, Oxon, OX11 OQX. Telephone: (0235) 446397.

Optics and Lasers in Engineering **9** (1988) 64–67

Announcements

SPIE 32ND ANNUAL INTERNATIONAL TECHNICAL SYMPOSIUM ON OPTICAL & OPTOELECTRONIC APPLIED SCIENCE AND ENGINEERING, 14–19 AUGUST 1988, SAN DIEGO, CALIFORNIA, USA

This symposium will comprise of twenty three conferences, a series of education courses, an instrument exhibit and a number of demonstrations. Topics to be covered include:

—Optical materials
—Infrared technology and cryogenic systems
—Optical and optomechanical technologies
—Information processing
—Photo-optical instrumentation engineering
—X-ray instruments, multilayers and sources.

Further information is available from:

SPIE,
PO Box 10,
Bellingham,
Washington 98227-0010,
USA

EUROSENSORS II AND THE 4TH SYMPOSIUM ON SENSORS & ACTUATORS, 2–4 NOVEMBER 1988, UNIVERSITY OF TWENTE, THE NETHERLANDS

The emphasis of this conference will be on sensor research. The programme includes plenary as well as parallel sessions, poster sessions, informal workshops and a small exhibition of commercial products. The conference language will be English. Further information is available

Optics and Lasers in Engineering (9) (1988)—© 1988 Elsevier Applied Science Publishers Ltd, England. Printed in Northern Ireland

from:

Eurosensors II,
PO Box 613,
7500 AP Enschede,
The Netherlands

IMAGE PROCESSING AND SYSTEMS CONFERENCE, 15–17 NOVEMBER 1988, KENSINGTON EXHIBITION CENTRE, LONDON, UK

The Image Processing and Systems Conference, run in conjunction with the Image Processing and Systems Exhibition, provides a unique opportunity for the presentation of the latest developments in Image Processing and Systems.

The Conference is directed at the needs and interests of professional engineers engaged in the development and exploitation of image processing. In addition, the Conference will provide a valuable forum for designers and manufacturers of systems and users to meet and exchange information on the latest technology.

Conference topics include;

—Image processing systems
—Underlying principles of image processing and analysis
—Image processing techniques
—Software and algorithms for image processing
—Dedicated image processors and integrated circuits
—Applications, including industrial, aerospace and defence, medical, security surveillance, automatic recognition, robot vision, speech recognition, processing and synthesis, acoustic signal processing.

Further information is available from:

Conference Chairman
Professor R. L. Grimsdale, School of Engineering and Applied Sciences, University of Sussex, Brighton, BN1 9QT, UK. Tel: (0273) 678047; Telex: 878358; Fax: (0273) 678335.

6TH MEETING OF OPTICAL ENGINEERING IN ISRAEL, 19–21 DECEMBER 1988, TEL AVIV, ISRAEL

This meeting will provide a forum in which various topics related to optics and electro-optics will be presented. An exhibition related to the

meeting topics will take place. The official language of the meeting is English. The following topics will be covered:

—Optical non-destructive industrial inspection
—Lasers for medical use
—Atmospheric transmission
—Optics for solar energy
—Optical design and fabrication
—Infrared technology.

Further information is available from:

Ortra Ltd,
PO Box 50432,
61500 Tel Aviv,
Israel,
Tel 972-3-664825

FRINGE ANALYSIS 89, AN INTERNATIONAL CONFERENCE, 3–6 APRIL 1989, SOUTHAMPTON UNIVERSITY, UK

The 4th annual meeting of the Fringe Analysis Special Interest Group organised by the Fringe Analysis Special Interest Group (FASIG) and the Institute of Sound and Vibration Research (ISVR) will be a major international conference devoted to state of the art techniques in generation and analysis of fringe patterns and interferograms. The programme will include tutorials, an equipment exhibition, company presentations of new technology and technical sessions with invited and contributed papers. Visits will be arranged to research laboratories at the ISVR and the near-by CEGB.

Authors from Industry and Academe are vinited to submit papers on 'applications and techniques of fringe generation and analysis'. Of particular interest are applications of Classical Interferometry, Holography, Speckle Interferometry, Speckle photography and PIV, Moiré and structured lighting techniques.

Abstracts should be returned by 31st August August 1988 to the address below. Full papers will be required by February 1989.

Dr N. Halliwell,
ISVR, Tizard Bldg,
University of Southampton,
Southampton SO9 5NH, UK

4TH CONFERENCE ON SENSORS AND THEIR APPLICATIONS, 25–27 SEPTEMBER 1989, UNIVERSITY OF KENT AT CANTERBURY, UK

Following the previous conferences in this series, the 4th Conference on Sensors and their Applications will be organised by The Instrument Science and Technology Group of The Institute of Physics. The event will be co-sponsored by a number of organisations such as The Institution of Electrical Engineers and The Institute of Measurement and Control.

The scope of the conference will cover all aspects of sensor research, development and applications. The programme will include plenary and parallel technical sessions together with poster sessions. Workshops dealing with important topics will be a feature of the Conference. A small commercial exhibition for sensor users and manufacturers is planned.

Contributed papers should be received before 1 April 1989. Bound copies of extended abstracts will be available to attendees.

Further information is available from:

The Meetings Office,
The Institute of Physics,
47 Belgrave Square,
London,
SW1X 8QX, UK

Optics and Lasers in Engineering **9** (1988) 68–70

Book Reviews

Gas Flow and Chemical Lasers. Edited by S. Rosenwaks. Proceedings of the 6th International Symposium, Jerusalem, September 8–12 1986, Springer-Verlag. Price: DM 120.

Proceedings of conferences can be disappointing, either because they appear too late to be useful or when the editing has been inadequately performed and, of course, if it has been a dull meeting neither speed nor perfect editing can make it exciting. These proceedings avoid most of the pitfalls, for this must have been an exciting symposium and the editor has done an excellent job to produce a very useful book just over a year later. By using the simple idea of arranging the papers in a logical form, Professor Rosenwaks has to a large extent overcome the staccato form of most multi-author texts. Thus we move from fundamental issues of fluid mechanics and optics through information on gas lasers set in wavelength order from the XUV to the infrared. This is followed by diagnostics, interaction with materials, propagation and applications. The volume ends with recent developments and a very interesting section on short-wavelength chemical lasers. Indeed, if it were not for the inevitable variety of typescript, one could at times forget that this was a conference so well do some of the papers run into the following one. Colin Webb from Oxford might not agree! His really excellent paper on metal vapour lasers, including their exciting medical applications, is immediately after one from the SDI organisation.

Obviously readers will find some papers more useful than others. I will keep returning to the invited papers as useful reference sources and I particularly enjoyed learning more about very short wavelength lasers and the possibilities for visible and near-infrared chemical lasers. It would be invidious to pick out particular papers for there are so many excellent ones, and in the entire volume of 80 papers in nearly 600 pages I failed to fine one that did not interest me. At less than £50·00 this book is, by modern price standards, an excellent buy. The diagrams and photographs are very well reproduced throughout and my only

Optics and Lasers in Engineering (**9**) (1988)—© 1988 Elsevier Applied Science Publishers Ltd, England. Printed in Northern Ireland

complaint is that some of the papers use too small print—or perhaps it is time for new reading glasses?

Maurice Kimmitt

Tunable Solid-State Lasers II. Edited by A. B. Budgor, L. Esterowitz, and L. G. DeShazer, Springer-Verlag, 1987. 368 pp. Hardback price: DM 90.

This text is the proceedings of the Optical Society Topical meeting from Zigzag, Oregon USA, June 1986. As the title of the book suggests, this is the second volume, the first being the proceedings from La Jolla, California, USA in 1984. Being a proceeding precludes any real editorial style and consequently the book is simply a compilation of papers. There are 10 chapters to the book dealing with aspects of solid state lasers and specific types. The book is basically split into three parts, the first two are major sections dealing with specific techniques and laser types, with a final application section finishing off the text.

Unfortunately there is no introductory chapter from the editors to set the scene for the reader and the first chapter launches straight into Spectroscopy. Papers presented describe two photon spectroscopy, spectroscopic measurements on laser materials and the use of spectral holeburning. This last paper suggests that photostability of certain ions may be strongly host-dependent. Chapter II looks specifically at the role of chromium doping, in particular the spectrographic analysis of this doping compared with other material and the effects of the choice of host crystal material.

Chapter III deals with certain theoretical aspects of crystal growth, growing techniques and post growth crystal treatments.

The second section deals with laser types and specifically considers the following materials: Chapter IV—Chromium Tunable Lasers, Chapter V—Alexandrite, Chapter VI—Titanium Sapphire, Chapter VII—Colour Centre, Chapter VIII—Rare Earth and Chapter IX—Neodymium.

The final chapter, Chapter X, deals with a broad range of papers dealing with the applications and non linear optics.

To summarize, the book is not aimed as a general text. Its contents are highly specific and should be of interest to those working in this field.

John Tyrer

What Every Engineer Should Know About Lasers. By D. C. Winburn, Marcel Dekker, New York, 1987, ISBN 0-8247-7748-4, 198pp. Price: $39.

The formulation of a comprehensive handbook for the non-specialist, non-physicist covering a topic which is now so diverse as laser technology, is a somewhat daunting task. Dr Winburn has produced a volume which is indeed comprehensive since it begins with the physical basis of lasers, reviews the various types which are in use and under development, and goes on to discuss laser applications in all their diversity.

From a practical viewpoint, perhaps the best part of the book is devoted to laser safety; in itself, the very presence of such a section demonstrates both the growing maturity of the laser business itself and the extent to which the author's attitudes are rooted in the practicalities of actually using lasers.

Having said that, one might criticise the overall emphasis of the application sections, since the role of lasers in surveying, and in control of tunnelling machinery is scarcely given adequate treatment compared to some of the more exotic prospects.

Any book of this nature is unlikely to be read cover-to-cover, at least in the first instance; it is a book for selective consultation and in this respect Dr Winburn has excelled himself. Whether one's interest is primarily in medicine, photochemistry, military devices or even art shows, the appropriate section is available for perusual. All-in-all a worthwhile laser primer.

C. A. Walker

INSTRUCTIONS TO AUTHORS

Submission of papers

Papers should contain work not published in full elsewhere. Short notes are acceptable and review articles may also be published at intervals, but the subject and content of the latter should first be discussed with one of the Editors. Manuscripts for consideration can be sent to either of the Editors, Professor F. P. Chiang or Mr G. T. Reid.

Types of contributions

Original papers; review articles; case studies; short communications; reports of conferences and meetings; book reviews; letters to the editor.

Manuscripts

Submission of a manuscript implies that it is not being considered contemporaneously for publication elsewhere. Three copies should be provided, in double-spaced typing on pages of uniform size, with a wide margin at the left. Generally the size of the manuscript should not exceed 6000 words or about 18 double-spaced pages of typescript, including diagrams and tables. Each paper should be provided with an Abstract of about 100–150 words, reporting concisely on the purpose and results of the paper.

The SI system should be used for all scientific and laboratory data; if, in certain instances, it is necessary to quote other figures, these should be added in parentheses. Temperatures should be given in Celsius. The unit billion (10^9 in America, 10^{12} in Europe) is ambiguous and must not be used. The use of proprietary names should be avoided. Papers essentially of an advertising nature will not be accepted.

References

References to published work should be given in the text by superscript numerals, with a reference list in numerical order at the end of the article. The list should give name(s) and initial(s) of author(s), exact title of paper, contracted title of periodical, single underlined, as in World List of Scientific Periodicals 4th Edn (1963–65), volume number in arabic numerals, double underlined, year of issue in parentheses and initial and final page numbers of article. The titles of books should be underlined, followed by the publisher, and the town and year of publication. Where appropriate, initial and final page numbers and the name(s) of the Editor(s) should also be quoted. References to unpublished data or private communications will not be accepted.

Illustrations

The original and one copy, which may if convenient be a photocopy, of each illustration should be provided. Line drawings should be in a form suitable for reproduction, in Indian ink, with stencilled lettering, etc. completed (avoid using dry transfer or typewritten lettering) and they should preferably all require the same degree of reduction. The type area of the journal is 123 mm wide by 193 mm deep. Photographs should be submitted as clear black and white prints on glossy paper. Each illustration must be clearly numbered and the title of the paper written on the reverse side.

Proofs

The author (or one selected author where several are involved) will receive proofs for perusal which must be returned within one week of receipt. New material or corrections which depart from the original manuscript will only be accepted at the discretion of the Editors. All joint communications must indicate the name and full postal address of the author to whom proofs should be sent.

Page charges and offprints

There are no page charges. 25 offprints of each article are supplied free of charge. Additional offprints can be ordered at current printing prices.

SUBSCRIPTIONS

1988—Two volumes, four issues per volume. Subscription price (Volumes 8 and 9): UK delivery, £148.00; Overseas delivery, £163.00/US$310.00. The £ Sterling price is definitive, US $ prices are subject to exchange rate fluctuation. All prices include postage and packing. All journals are distributed worldwide by air-speeded delivery at no extra cost to the subscriber. Subscription orders should be addressed to:

Elsevier Applied Science Publishers Ltd, Crown House, Linton Road, Barking, 'Essex IG11 8JU, England

In the United States and Canada: For further information contact Elsevier Science Publishers, Journal Information Center, 52 Vanderbilt Avenue, New York, NY 10017, Tel. (212) 916–1250.

ELSEVIER APPLIED SCIENCE PUBLISHERS LTD
Crown House, Linton Road, Barking, Essex IG11 8JU, England

OPTICS and LASERS in ENGINEERING

VOL. 9 NO. 1 1988

(Abstracted/indexed in: *Current Contents*; *Metals Abstracts*; *Photographic Abstracts*; *Physics Abstracts*; *Science Citation Index*)

CONTENTS

Effects of Plasma on CO_2 Laser Cutting Quality 1
B. S. YILBAŞ & Z. YILBAŞ (Turkey)

Use of a CO_2 Laser for Thermal Effect Simulation on Sintered Carbide Inserts 13
O. DE PASCALE, C. ESPOSITO, M. LEPORE, S. LO CASTO & G. PASSANNANTI (Italy)

The Preheating Temperature Parameter for Deep Penetration Welding With High Energy Focused Beams 23
R. PERETZ (FRG)

A Differential Interference Contrast System Incorporating a Murty Interferometer and Holographic Correction 35
K. MATSUDA, M. NAMIKI & T. H. BARNES (Japan)

Frozen Strain Moiré Used in the Analysis of Impact Loading 47
J. W. TONG, H. Q. LI & Y. Q. JIA (Peoples Republic of China)

Research Note

Designed Experiments with a Laser Dilatometer 57
P. SHARLANDJIEV & A. SLAVTCHEVA (Bulgaria)

Conference Report 61

Announcements 64

Book Reviews

Gas Flow and Chemical Lasers. Edited by S. Rosenwaks. Proceedings of the 6th International Symposium, Jerusalem, September 8–12 1986, Springer-Verlag 68
(Reviewed by Maurice Kimmitt)

Tunable Solid-State Lasers II. Edited by A. B. Budgor, L. Esterowitz and L. G. DeShazer, Springer-Verlag, 1987 69
(Reviewed by John Tyrer)

What Every Engineer Should Know About Lasers. By D. C. Winburn, Marcel Dekker, New York, 1987 70
(Reviewed by C. A. Walker)
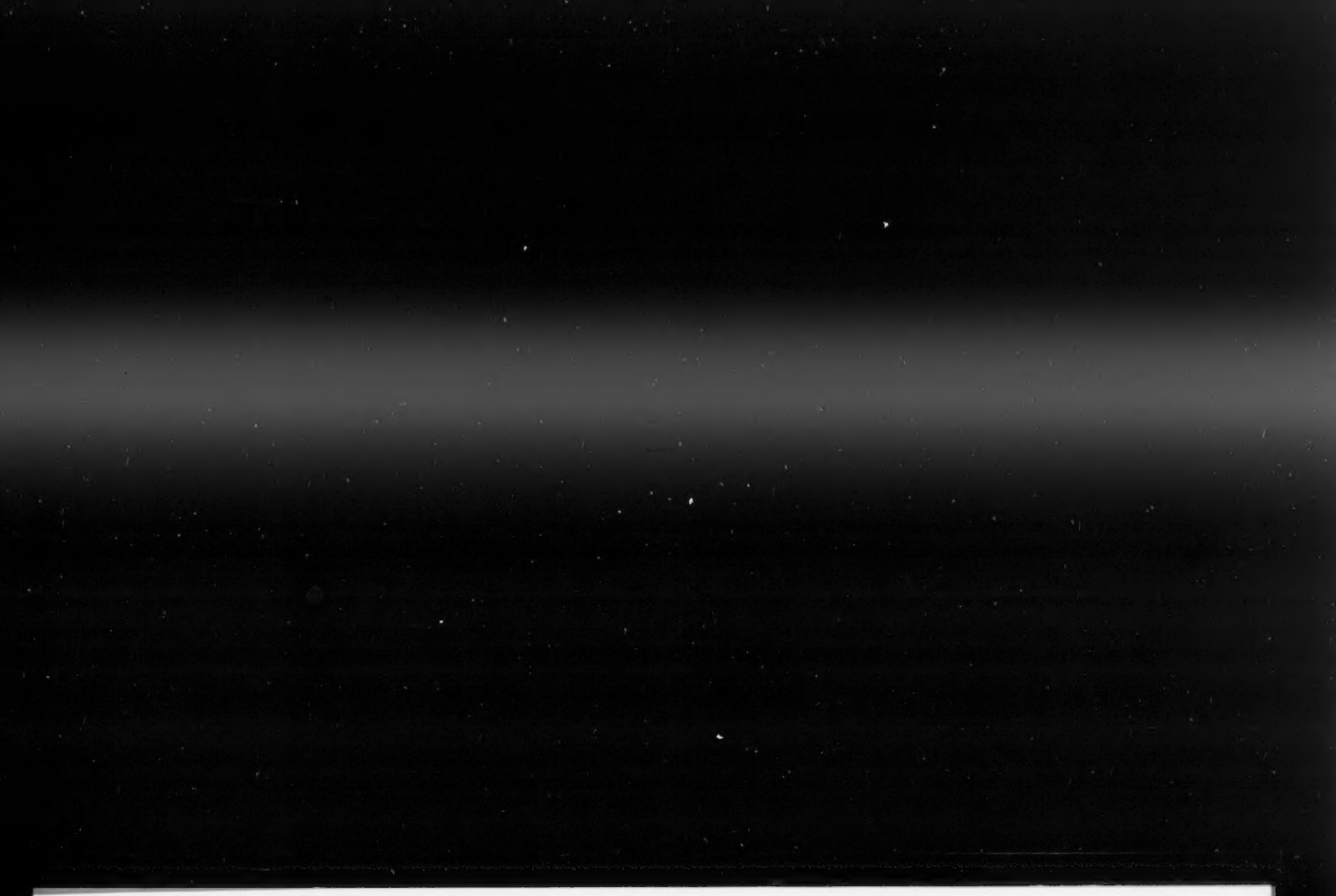
ELSEVIER APPLIED SCIENCE